ISTANBUL TECHNICAL UNIVERSITY ★ INSTITUTE OF SCIENCE AND TECHNOLOGY

MIXED LUBRICATION ANALYSIS OF LASER TEXTURED CYLINDER BORES

M.Sc. Thesis by

O. Taha ŞEN, B.Sc.

Department : Mechanical Engineering

Programme: Automotive

JUNE 2007

ISTANBUL TECHNICAL UNIVERSITY ★ INSTITUTE OF SCIENCE AND TECHNOLOGY

MIXED LUBRICATION ANALYSIS OF LASER TEXTURED CYLINDER BORES

M.Sc. Thesis by

O. Taha ŞEN, B.Sc.

(503051710)

Date of Submission: 07 May 2007

Date of Defense Examination: 08 June 2007

Supervisor (Chairman):   Assist. Prof. Dr. Özgen AKALIN

Members of the Examining Committee: Prof. Dr. Metin ERGENEMAN (İ.T.Ü.)

Prof. Dr. Mustafa ÜRGEN (İ.T.Ü.)

JUNE 2007

İSTANBUL TEKNİK ÜNİVERSİTESİ ★ FEN BİLİMLERİ ENSTİTÜSÜ

**LAZER İLE İŞLENMİŞ SİLİNDİR YÜZEYLERİNİN
KARMA YAĞLAMA REJİMİNDE İNCELENMESİ**

**YÜKSEK LİSANS TEZİ
Müh. O. Taha ŞEN
(503051710)**

**Tezin Enstitüye Verildiği Tarih : 07 Mayıs 2007
Tezin Savunulduğu Tarih : 08 Haziran 2007**

Tez Danışmanı: Y. Doç. Dr. Özgen AKALIN
Diğer Jüri Üyeleri: Prof.Dr. Metin ERGENEMAN (İ.TÜ.)

Prof.Dr. Mustafa ÜRGEN (İ.T.Ü.)

HAZİRAN 2007

ACKNOWLEDGEMENT

TABLE OF CONTENTS

ABBREVIATIONS

CA	**: Crankangle**
LST	**: Laser Surface Texturing**
FE	**: Finite Element**
FDM	**: Finite Differencing Method**
BDC	**: Bottom Dead Center**
TDC	**: Top Dead Center**
EHD	**: Elastohydrodynamic**
FTDC	**: Firing Top Dead Center**
TDI	**: Turbo Direct Injection**
CSEM	**: Centre Suisse d'Electronique et de Microtechnique**
IFAS	**: Institut für Fluidtechnische Antriebe und Steuerungen**
IPT	**: Institut Produktionstechnologie**

LIST OF TABLES

LIST OF FIGURES

LIST OF SYMBOLS

b	: Effective Ring Length
c	: Nominal Radial Clearance
h	: Nominal Film Thickness
h$_{dimple}$	: Dimple Profile
h$_{max}$	: Mean Local Film Thickness
h$_T$	: Mean Local Film Thickness
i,j	: Nodal Coordinates
n	: Running Speed
p	: Pressure
p$_1$	: Inlet Pressure
p$_2$	: Outlet Pressure
p$_b$	: Back Pressure
r	: Crank Radius
x$_1$	: Lubrication Start Point
x$_2$	: Film Rupture Point
x$_3$	: Film Formation Point
x$_4$	: Lubrication End Point
A$_1$, A$_2$, A$_3$	: Parameters for Shear Flow Factor
C,r	: Parameters for Pressure Flow Factors
C$_{i,j}$, S$_{i,j}$	: Coefficients of Discretized Reynolds Equation
E$'$	: Composite Young Modulus
F$_t$	: Ring Tension Force
F$_g$	: Gas Force
F$_{hyd}$	: Hydrodynamic Force
F$_c$	: Asperity Contact Force
H	: Non-dimensional Film Thickness
H$_\sigma$	: The Ratio of Local Film Thickness to Composite Surface Roughness
K$'$	: Parameter for Asperity Contact Model
P	: Non-dimensional Pressure
S	: Sommerfeld Number
T	: Non-dimensional Time
U	: Sliding Speed
U*	: Non-dimensional Sliding Speed
V$_{r1}$, V$_{r2}$	: Surface Roughness Variance Ratios
W	: Specific Load
X, Y	: Non-dimensional Coordinates
α$_1$, α$_2$	: Parameters for Shear Flow Factor
β	: Squeeze Film Factor
β$'$	: Asperity Radius of the Curvatures
δ$_1$, δ$_2$	: Surface Roughness Profiles
φ$_c$	: Contact Factor
φ$_s$	: Shear Flow Factor

φ_x, φ_y	**:** Pressure Flow Factors
γ	**:** Peklenik Factor
λ	**:** Film Thickness Ratio
μ	**:** Dynamic Viscosity
ν	**:** Poisson's Ratio
σ	**:** Composite Surface Roughness
σ^*	**:** Non-dimensional Composite Surface Roughness
σ_1, σ_2	**:** Surface Roughness for Sliding Surfaces
ω	**:** Crank speed

MIXED LUBRICATION ANALYSIS OF LASER TEXTURED CYLINDER BORES

SUMMARY

This study aims to investigate the tribological performance of a piston ring which reciprocates in a laser surface textured cylinder bore. For this purpose a detailed ring dynamics model is constructed and the problem is solved with a code which is prepared with MATLAB. In the solution of the problem modified Reynolds equation which contains flow factors is used and therefore the asperities of the ring and the bore are added to the model. Furthermore an asperity contact model is added for very little clearances between the ring and the bore and this makes the model to work in both mixed and hydrodynamic lubrication regimes. The modeling of the rupture of the lubricant film between the clearance of the ring and the bore, Reynolds boundary conditions is used and by the help of this, rupture boundary of the lubricant film is calculated. Thus there are small dimples on the bore which are created with laser surface texturing technique, a floating bore surface is constructed and the solution is done for every crankangle.

As a result, a comparison between the tribological performance of conventional and laser surface textured cylinder bores is done. Furthermore a discussion is done about the tribological performance of laser surface textured cylinder bores with different specifications. Moreover surfaces with different dimple shapes are also solved and discussed.

LAZER İLE YÜZEY İŞLEMEYE TABİ TUTULMUŞ SİLİNDİRLERİN KARMA YAĞLAMA REJİMİNDE ANALİZİ

ÖZET

Bu çalışmanın amacı lazer ile yüzey işlemesine tabi tutulmuş silindir duvarı ile üzerinde öteleme hareketi yapan piston segmanının tribolojik performansını incelemektir. Bu amaçla detaylı bir segman dinamiği modeli oluşturulmuş ve oluşturulan modelin ışığı altında MATLAB dilinde hazırlanan bir kod ile problem çözülmüştür. Problemin çözümünde silindir duvarı ve piston segmanı üzerindeki yüzey pürüzlülüklerini modele katabilmek için akış faktörlerini içeren değiştirilmiş ortalama Reynolds denklemi kullanılmıştır. Ayrıca segman ve silindir duvarı arasındaki aralığın çok düşük olduğu durumlar için yüzey pürüzlülüğü temas kuvveti altprogramı ana koda eklenmiştir ve bu sayede model hem karma hem de hidrodinamik yağlama rejimlerinde çalışır hale getirilmiştir. Yağlama bölgelerindeki yağ filminin kopmasının modellenmesinde ise Reynolds sınır koşulları kullanılmış ve yağ filminin kopma sınırı belirlenmiştir. Lazer ile işleme sonucunda oluşan gözeneklerin silindir üzerinde olmasından ve segmanın silindir önündeki öteleme hareketinden dolayı hareketli bir silindir modeli kurulup her krank açısı için çözüm yapılmıştır.

Sonuç olarak konvansiyonel ve lazer ile işlenmiş silindirlerin tribolojik performansları açısından karşılaştırması yapılmıştır. Bundan başka farklı lazer ile yüzey işleme spesifikasyonuna tabi tutulmuş ve farklı şekil ve boyutlardaki gözeneklerin yağlama üzerine etkileri tartışılmıştır.

1 INTRODUCTION

The critical issues about the environment at the second half of the 20th century pushed the engine manufacturers to design and construct more fuel efficient and compact engines. Although this can be obtained in several ways, increasing specific loads, speeds and temperatures for the major frictional components of the engine which are the piston assembly, the valve train and the journal bearings and decreasing the viscosity of the engine lubricants are the main issues in tribological meaning. But these modifications lead to a decrease at the lubricant film thicknesses between the mating surfaces of these components and the role for the topography and surface profile of the two surfaces in determining tribological performance becomes more crucial [1].

As it is known, the total fuel energy cannot be taken as output energy from an internal combustion engine and there are several components of this power loss like heat, mechanical and pumping losses. About this topic Akalın and Newaz claims that the significant part of the total power loss is because of the piston ring and cylinder bore friction in a reciprocating engine [2]. Also some studies which is done on a medium size passenger car during an urban cycle shows that only 12% of the available energy in the fuel is being spent to the driving wheels. It is also found that 15% of the total fuel energy is being lost mechanically, especially as frictional losses. Furthermore, Rohde claims that approximately 15 – 25% of the net heat energy which is potentially available to propel an automobile is expended in engine mechanical friction and the friction at the piston ring cylinder interface forms the 25 – 50% of this total mechanical loss [3]. Figure 1.1 shows the distribution of the power losses in an internal combustion engine.
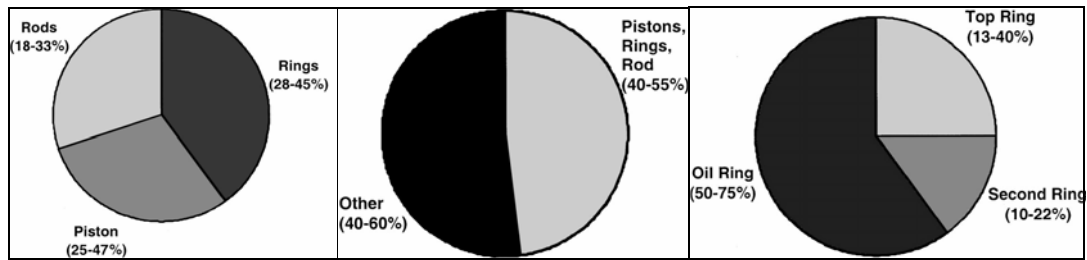
Figure 1.1 Power Loss Distribution in an Internal Combustion Engine [4]

1.1 Effects of Piston Ring Dynamics on Engine Performance

The main functions of a piston ring can be described as to seal off the combustion pressure, to distribute and control the oil on the cylinder bore, to stabilize and help the cooling of the piston and these requirements on the ring pack is related to the ring dynamics [5]. Ring dynamics which contain radial and axial ring motion and ring twist motion affect the operation of the ring, the oil film formation on the cylinder bore, the friction between the ring and the bore, the wear of the ring and cylinder bore and the blow-by across the ring pack. Also, the dynamic performance of the rings affects the economy index, service lives and emission characteristics of the internal combustion engines [6].

The effects of piston ring dynamics on the performance of an internal combustion engine can be summarized in four main topics which are friction, wear, blow-by and oil consumption.

With the decrease of the lubricant film between the piston ring and cylinder bore, asperity contacts occur at the interface and as a result of these contacts wear patterns start to develop on the surfaces. According to Yong et al., wear of the cylinder bore determines the service lives and many of running faults are due to the failure of ring-liner pair [6].

Blow-by, which is known as the gas transition from combustion chamber to crankcase, affects the performance of the engine significantly. As a result of the gas transition from combustion chamber to crankcase, the combustion chamber pressure decreases and this causes a decrease at the power of the engine.

As a last parameter ring dynamics affect oil consumption through some different oil consumption mechanisms like scraping of the oil by the top ring, blowing of the oil through the top ring end gap. As a result of this, oil consumption, which increases the

emission values, becomes a major task in the development process of modern diesel engines [7].

1.2 Parameters Effecting Ring Motion

The main parameters which are effective on the ring motion can be given as piston secondary dynamics, interring pressures and ring face profile geometry.

Piston secondary dynamics, which can be defined as the lateral and tilt motion of the piston inside the cylinder bore, affect the piston ring motion in terms of its tilt motion. As a result of this motion, piston rings also rotates and the interface between the piston ring and the cylinder bore becomes different, and so the lubrication characteristics and forces acting on the piston ring changes [5].

The second one, which is the interring pressures, affects ring motion in terms of ring flutter which means the rapid up-an-down movement of the ring in the groove. As it is clear ring moves to the lower pressurized part of the groove because of the higher pressure at the other side and if the change of these pressures occurs very rapidly in an engine cycle the ring makes a flutter motion. This motion is not desired and it contributes to pressure leakage from the combustion chamber [8].

As a result of the change of ring face profile geometry, the lubricant film thickness distribution changes at the cylinder bore and piston ring interface. As an example there are several piston rings that have different face profiles like taper faced, keystone, half keystone and barrel shaped (Figure 1.2) and the lubrication characteristics of them are also different [5]. For example rectangular shaped ring satisfactorily meets the sealing demands but it also increases the force distribution at the face of the ring. Although the barrel shaped piston rings has a worse sealing property, the total force acting from the ring face is lower than the rectangular shaped ones, because with this geometry the compression pressure is able to act from the face side and it counteracts some of the ring tension force. Also a taper faced piston ring has good oil scraping ability and it enables the compression gas pressure to act from the face side. As a result of this taper faced piston ring helps to relieve the pressure against the liner wall and reduces the wear rate.
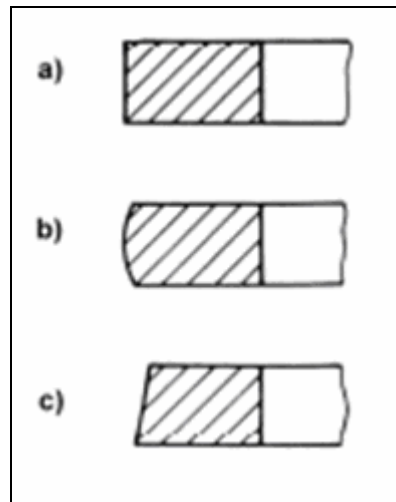
Figure 1.2 Ring Profiles a) Rectangular Shaped b) Barrel Shaped c) Taper Faced

1.3 Laser Surface Texturing

In practical usage there are several surface finishing techniques like honing, lapping, etching, ion beam texturing etc. In honing process, abrasive stones are used to remove the asperities from the surface they are working on. Lapping is also another machining process in which two surfaces are rubbed together with an abrasive between them. This technique enables to have very accurate surfaces and to obtain a specific surface roughness. Etching is a surface preparation of metal by a chemical process and removal of a layer of the base metal. In ion beam texturing process a mask is used to create a pattern on the substrate and surface material from the unmasked areas are removed. This method is accomplished using a high energy beam to selectively remove material from the substrate. Although, these techniques are still in usage, laser surface texturing is considered as the most recent surface finishing technique. According to Etsion [9] fast processing times, controllability of the shape and size of the dimples and cleanliness to the environment makes this technique the most promising concept. Also controllability of this technique which means ability to apply different dimple shapes and sizes (Figure 1.3) makes the optimization for the best lubrication performance easier.

Thus LST is the most promising technique, many researchers study on this topic all over the world in order to apply it on many mechanical components. As an example, in Germany University of Erlangen-Nuremberg, IFAS/IPT Aachen, University of Hannover and Gehring; in Israel SurTech; in Japan Tohoku University; in China East China University; in Switzerland University of Bern and CSEM; in USA Argonne

National Laboratory, Western Michigan University and Stein Steel Company; in Russia General Physics Institute Moscow and in France Mediterranean University can be given as the main research locations about LST [9].
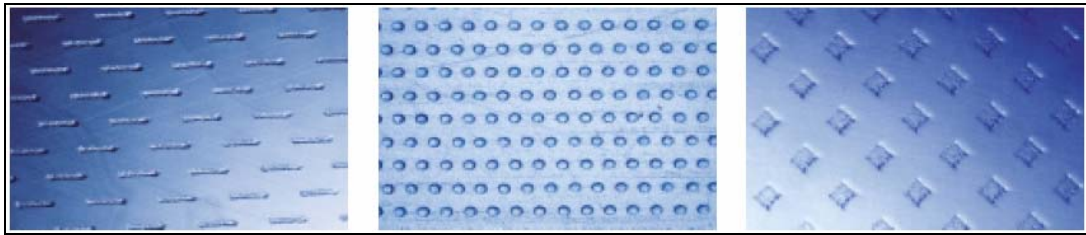
Figure 1.3 Different Dimple Shapes [11]

Commercially there is only one study in the literature which was done on an Audi four cylinder 1.9 liter TDI diesel engine [10]. The surface treatment was done by a purpose-built workstation which incorporates with a high pulse energy Excimer laser which operates at a wavelength of 308 nm and pulse duration of 25 ns. The surface texturing was applied on the cylinder bore with laser beam and the laser beam was directed into the beam delivery optics. The final optic on this workstation was a turning mirror which sits inside the cylinder and directs the beam at the cylinder bore. In this workstation changing the height of this final optic allows to apply the process along the length of the cylinder bore and in circumferential direction rotating the cylinder block makes the process possible (Figure 1.4).
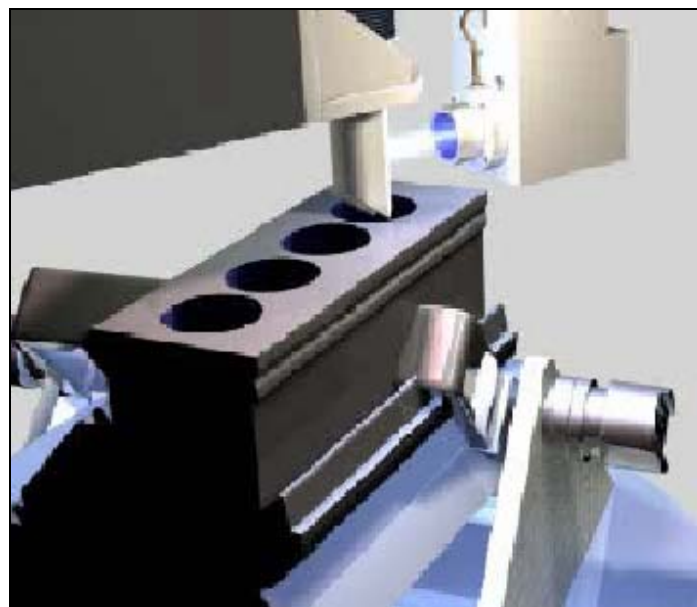
Figure 1.4 A LST Workstation Sample [12]

In this study, standard endurance protocols which are designed to simulate multiple duty cycles like, variable engine revolutions at full load endurance, variable engine revolutions/variable load, full load/low load and start/stop, were applied on these laser textured TDI engines. The engines were run for 602 hours and according to the tests the result were taken as in Figure 1.5.
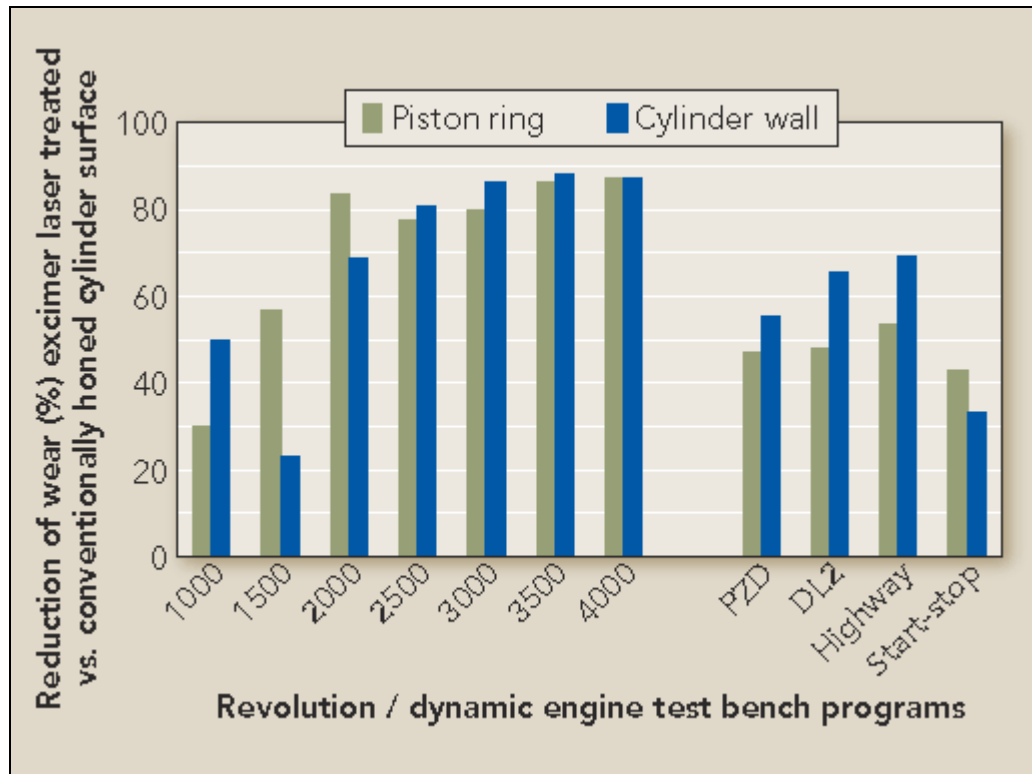
Figure 1.5 Test Results for LST [10]

As it is seen in Figure 1.5, LST yields to a significant decrease of wear on both cylinder bore and piston rings when compared to a mechanically honed cylinder bore.

In another study, [13] which was done on real engines, it was seen that LST helps to reduce the wear on both cylinder bore and piston ring and LST with pocket structure seems to be the best choice due to wear (Figure 1.6).
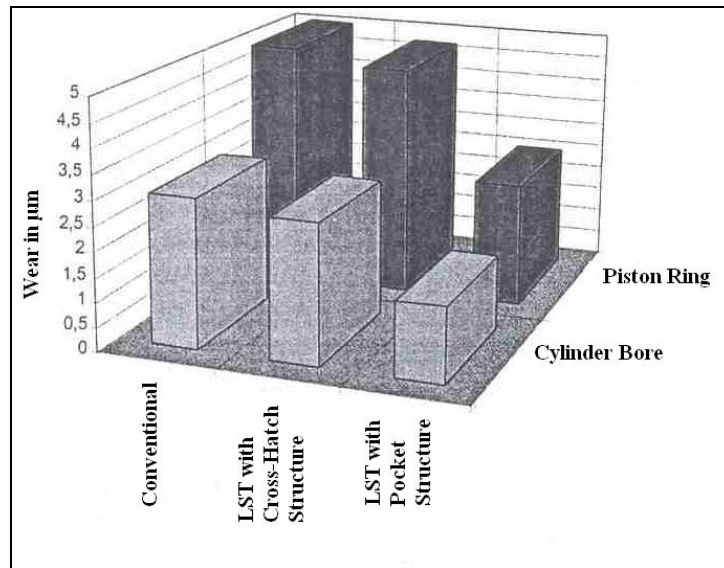
Figure 1.6 Piston Ring Cylinder Bore Wear Results [13]

The main idea is that the dimples which are created with LST behave like micro reservoirs and trap the oil inside of the dimple [10]. Thus these dimples are not interconnected, the oil cannot escape from the dimple and the ring hydroplanes on these trapped oil droplets. This mechanism is shown in Figure 1.7.
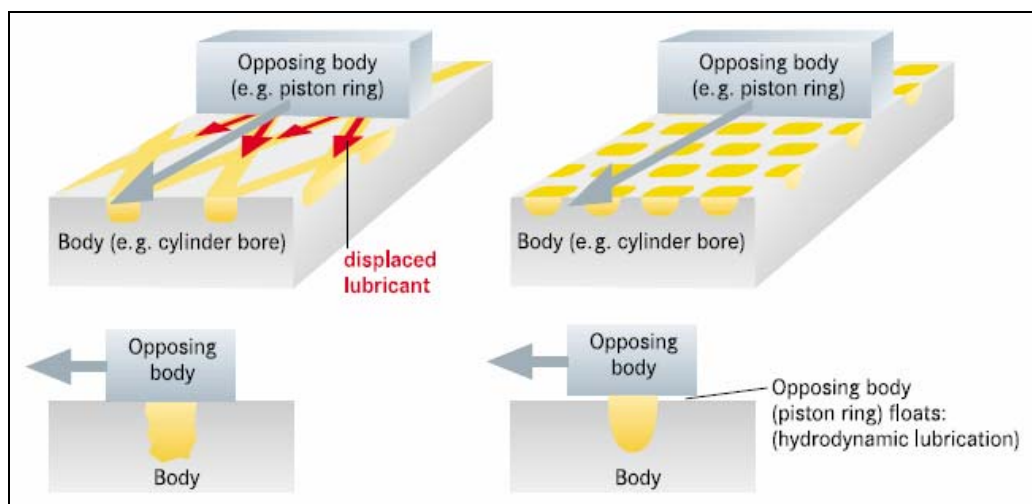
Figure 1.7 The Reason of Reduced Friction with LST [11]

1.4 Literature Survey

In literature, there are many studies about the effects of laser surface texturing on the tribological performances of bearings, piston ring-cylinder bore couples and test specimens etc. However the theoretical and experimental studies on piston ring cylinder bore couple are all done for laser surface textured piston rings, which means that the dimples doesn't change its place in the lubricated zone with the reciprocating

7

motion. In this part, these theoretical and experimental studies will be discussed with their results.

1.4.1 Theoretical Studies on Laser Surface Texturing

Wang and Zhu [14] studied the effects of design factors such as dimple size, depth and density on mixed lubrication performance of textured surfaces and showed results about design factors, operating conditions and interface status. According to their study, authors found that, at very small dimple sizes film thickness reduced with the increase of dimple size, but this trend turned back when the dimple size further increased. Furthermore, the investigation of the second design factor, which is dimple depth, showed that deeper dents yield more severe hydrodynamic reduction and contact ratio increases with depth and for dimple density investigation, it is found that 5% dimple density looks to be the best choice. According to this study, the authors claimed that surface topography and textures play a significant role and the microgeometry must be taken into account.

Feldman et al. [15] studied the validity of the Reynolds equation on textured parallel surfaces. In this study, the same problem was solved in two different methods which are software that uses Reynolds equation and ANSYS/Flotran package program that uses Navier-Stokes equations. The results were given for different dimple aspect ratios and dimensionless clearances. As a result, it was found that Reynolds equation gives acceptable result and it can safely be used for solving textured surfaces.

Ronen et al. [16] developed software in order to investigate the effect of surface texturing on lubrication. In this study, rings are modeled by two nominally flat surfaces and reciprocating relative to a flat surface that simulates the cylinder liner. As a result of this study, it was seen that interaction between adjacent dimples is significant and its effect on the hydrodynamic pressure distribution cannot be neglected, the variation in the friction force with the crank angle mainly depends on the variation of the sliding velocity, the area density of the dimples and the inertia of the rings have little effect on average friction force. Also authors claimed that there is an optimum value for the dimple depth over diameter ratio which yields to a minimum friction force and increasing the number of dimples over the axial length of the ring up to 12 reduces the friction sharply, but more dimples than 12 do not affect friction force too much. Although the model does not allow direct comparison with a

system that does not have dimples, the authors also claimed that a friction reduction of 30% and even more is feasible with textured surfaces.

Kligerman et al. [17] developed software in order to investigate the potential use of partial laser surface texturing to enhance friction reduction obtained with full laser surface texturing. The main goal of this study was to determine the optimum parameters of the partial LST for given engine structural and operating conditions and to investigate the engine structural and operating conditions on the friction losses between the piston ring and cylinder liner in the presence of partial surface texturing. As a result of this study, authors found an optimum value of textured portion and dimple depth and the position of the textured portion has little effect on the friction force. Also authors claimed that average friction force is not affected by the dimple diameter and the minimum average friction force for the optimum partially textured piston ring is significantly lower than that for the corresponding optimum fully textured ring.

Feldman et al. [18] analyzed the potential benefit of partial LST in a hydrostatic gas seal and developed a theoretical model in order to compare the lubrication performance of textured seal and an equivalent step seal. As a result of this study, authors found that the performance of partial LST hydrostatic gas seal is mainly dependent on the dimples area density and is not affected by the dimple diameter. Also, authors claimed that dimple depth has a very little effect on the performance of the partial LST seal and lubricant leakage through a partial LST seal is significantly less than that for the corresponding equivalent radial step seal.

Kligerman and Etsion [19] developed a FE model for a laser surface textured circumferential gas seal to evaluate the hydrodynamic effect of the surface texturing on the seal force balance. As a result of this study, authors found that the presence of the micro dimples on one of the seal mating faces generates substantial hydrodynamic effect and it maintains a small clearance between the rotating shaft and stationary seal ring. Also the results showed that texturing parameters can be optimized to get maximum hydrodynamic effect.

Brizmer et al. [20] developed a theoretical model for parallel thrust bearings in order to investigate the effects of full and partial laser surface texturing, where the application of LST on whole surface is called full LST and application on a portion

of the surface is called partial LST. Authors claimed that in full LST, cavitation occurs in each dimple and there is no interaction between adjacent dimples, but in partial LST there is a collective effect and interaction between adjacent dimples is significant. As a result of this study, authors found that full LST is not useful for developing the large load carrying capacity which is expected from a hydrodynamic thrust bearing. Authors also claimed that the collective effect of partial LST is capable of generating substantial load carrying capacity, approaching that of optimum conventional thrust bearings.

Siripuram and Stephens [21] developed a theoretical model in order to investigate the effect of deterministic asperity geometry on friction, leakage and film thickness for a given set of operating condition. Predominantly, authors were interested in asperity shape, orientation, size and distribution. Authors worked on seven different asperity geometries in both positive and negative configurations. As a result of this study, authors found that friction coefficient is largely independent of asperity shape and orientation but very sensitive to asperity area fraction. Also, it is found that leakage and film thickness are dependent on asperity shape, concavity, orientation and size.

1.4.2 Experimental Studies on Laser Surface Texturing

Ryk et al. [22] performed an experimental study to evaluate the effect of laser surface texturing in the form of micro dimples in reciprocating automotive components. In order to do this, authors designed a test rig in which two different test specimen configurations can be used, which are plane surfaces and a real ring/liner pair. As a result of the experiments it was found that 40% reduction on the friction is available for plane surfaces and 30% reduction is available for real ring/liner pair. Authors also obtained a good correlation with theoretical results from a model that simulates the plane surfaces configuration.

Etsion et al. [23] performed an experimental study on laser surface textured parallel thrust bearing and tried to show the correlation between experimental study and theoretical model. As a result of this study, good correlation was found with a theoretical model as long as the laminar flow in the fluid was valid. Also, it was found that clearance between mating surfaces was three times higher in partial LST and friction coefficient is lower in partial LST bearings.

Ryk et al. [24] made an experimental study in order to investigate the effect of partial LST on friction reduction in piston rings. Friction force measurements were done on a reciprocating test rig with parallel flat faces simulating flat piston rings and cylinder liner. The results were compared with untextured and full LST cases and partial LST showed the best performance in the reduction of friction force.

Kovalchenko et al. [25] performed an experimental study with a pin on disk apparatus at different sliding speeds, nominal contact pressures and lubricants with different viscosities. Test specimens used in this study were in different surface characteristics like non-textured, textured, grounded and polished. As a result of this study, authors found that LST expands the range of hydrodynamic lubrication regime in terms of load and sliding speed for both low and high viscosity lubricants. Also it was seen that LST reduces the friction coefficient when compared with untextured surfaces and lower area dimple density is more beneficial for lubrication regime transitions.

Wakuda et al. [26] performed an experimental study to clarify the potential of textured micro- dimples on a silicon nitride ceramic plate mated with cylindrical-shaped steel elements and the experiments were done with a unique pin-on-disk test rig. As a result of this study, authors found that surface texturing is very effective on friction reduction even under severe friction conditions and friction coefficient reduction is obtained without forming undesirable tribochemical films with a well-lubricated and textured sample. Also, authors claimed that the distribution of micro-dimples is also an important factor and the dimple geometry has little influence on the frictional properties regardless of rounded or angular profiles.

Mourier et al. [27] studied the effect of micro cavity on the lubrication of a circular elastohydrodynamic lubrication contact by both experimentally and theoretically. In their study, authors investigated the effect of micro cavity in pure rolling and rolling sliding conditions. As a result of this study, authors found that under pure rolling conditions the micro cavities do not affect the oil film thickness and when a sliding velocity is introduced, the lubricant film thickness distribution is disturbed by the passage of a micro cavity. The authors also claimed that deep cavities may cause a local decrease or collapse of the lubricant layer.

Kovalchenko et al. [28] designed an experimental study in order to investigate the effect of micro dimples on transition of lubrication regime from boundary to hydrodynamic by measuring the friction and electrical contact resistance in a pin on disk test system. Tests were done on different disk samples and with different speed, load and lubricant conditions. As a result of this study, authors found that surface texturing expands the range of hydrodynamic lubrication regime and reduces the friction coefficient. Also it was found that removal of the bulges which form after LST process at the edge of the dimples is essential in order to observe the positive impact of LST on hydrodynamic lubrication.

Etsion and Halperin [29] performed an optimization study of a partially laser surface textured mechanical seal, which is subjected to laser surface texturing over an annular portion of one of its mating rings, by theoretically and experimentally and theoretical and experimental results showed a good correlation. For the theoretical model, results showed that average pressure between mating surfaces is bigger in partially textured surfaces than untextured and fully textured surfaces and average pressure is independent of the clearance between the mating surfaces for partially textured surfaces. For the experimental study LST seals showed less friction torque than standard seals and it is seen that the pressure capability of the seal with LST is greater than the standard seal.

1.5 Objectives

As it can be seen through the literature survey, LST has significant advantages over conventional surfaces. Significant reduction of engine friction, wear and oil consumption can be obtained using this technique. However, lubrication characteristic of LST is not well known and because of this, the main objective of this study is to develop a computational method to investigate the tribological performance of a piston ring and LST cylinder bore couple. While doing this the results like the change of lubricant film thickness and asperity contact force will be compared for LST and conventional cylinder bores over whole engine cycle. Also the effect of dimples on the hydrodynamic pressure distribution will be examined.

2 THEORY

In this part of the study some theoretical information will be given.

2.1 Lubrication Theory

2.1.1 Lubrication Regimes

In lubrication theory, there are several regimes that differ from each other according to a number which is called Sommerfeld number. This number is derived in order to get a dimensionless parameter and it is described with dynamic viscosity (μ), sliding speed (N) and specific load (W) as in Figure 2.1.

$$S = \frac{\mu U}{W}$$
(2.1)
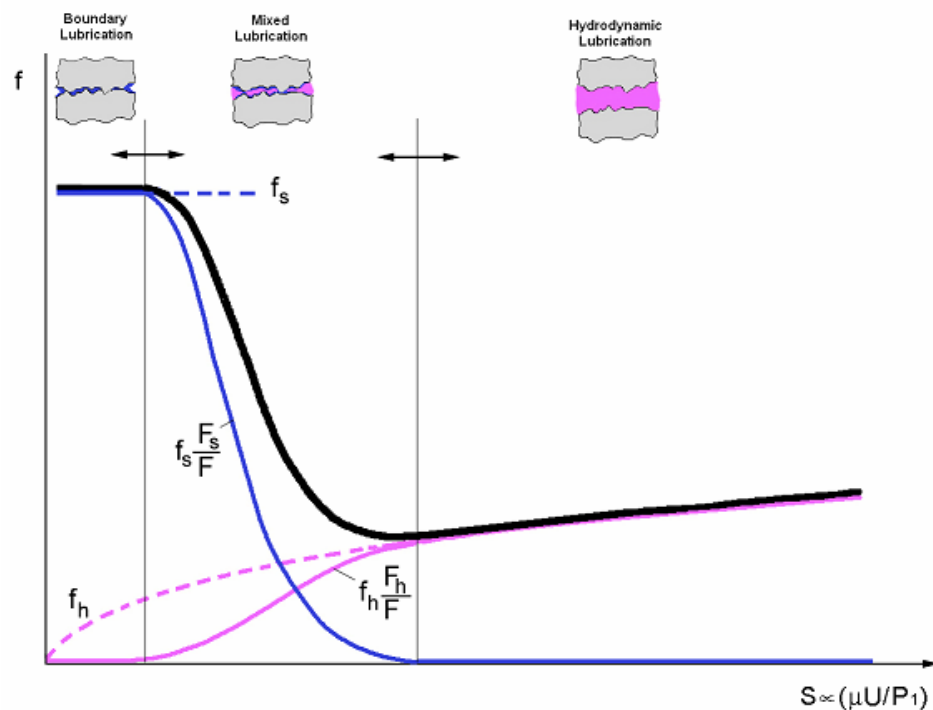
Figure 2.1 Stribeck Curve According to Sommerfeld Number

Later on this parameter was modified and film thickness ratio (λ), which is the ratio of effective film thickness to surface roughness, was started to be used in order to define the lubrication regimes [30] (Figure 2.2).
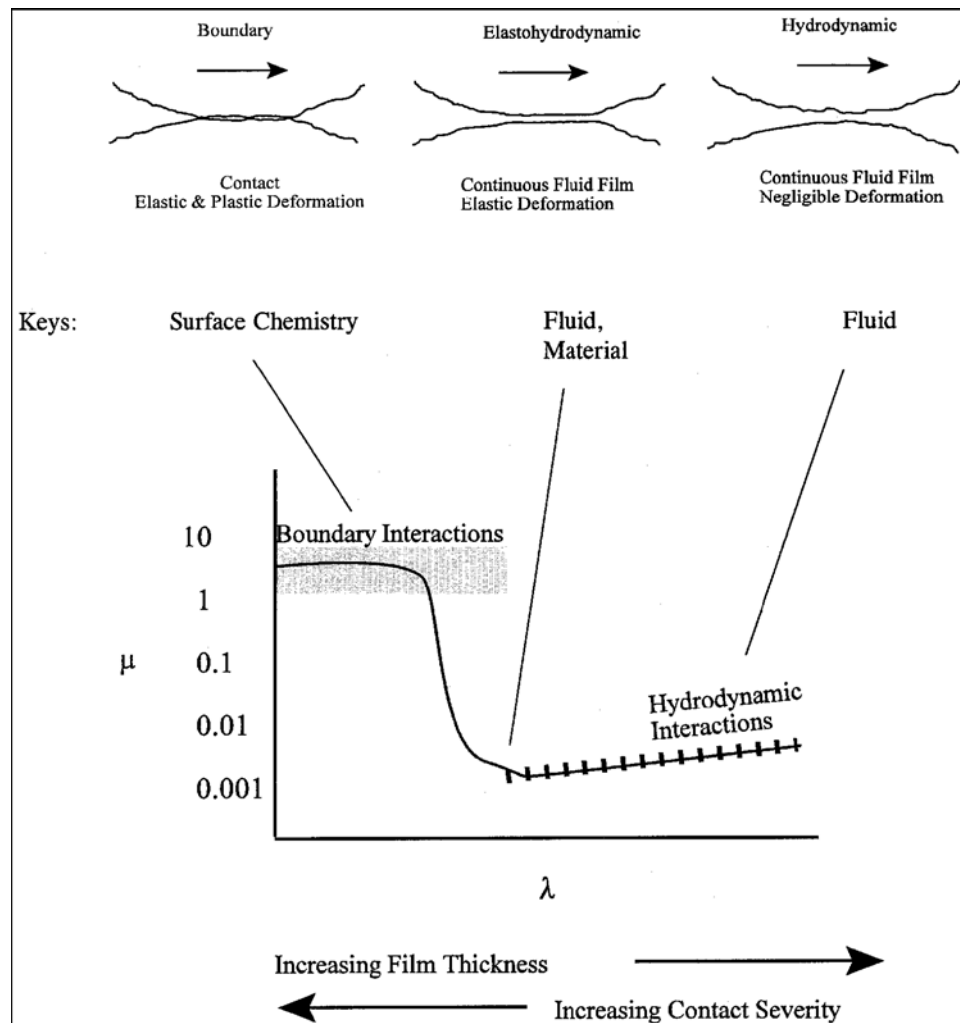
Figure 2.2 Stribeck Curve According to Film Thickness Ratio

According to film thickness ratio these lubrication regimes can be defined:

- Boundary Lubrication

- Mixed Lubrication

- Hydrodynamic Lubrication

- Elastohydrodynamic Lubrication

2.1.1.1 Boundary Lubrication

In many cases, boundary lubrication regime is defined as the critical lubrication regime that governs the life of the components subject to wear and this regime usually occurs under high load and low speed conditions in bearings, gears, cam and tappet interfaces, piston rings and liner interfaces, pumps, transmissions, etc.

The increase of the contact pressure beyond elastohydrodynamic lubrication conditions causes a plastic deformation at the contacting asperities and an increase at the number of the contacts as well as a decrease at the fluid film thickness. When the average fluid film thickness falls below the average relative surface roughness, surface contact becomes a major part of the load supporting system and mechanical interactions of these contacts produce wear, deformation, abrasion, adhesion, and fatigue under dry sliding conditions. Furthermore chemical reactions between the lubricant molecules and the asperity surface, due to frictional heating, often produce a boundary chemical film which can be either beneficial or detrimental in terms of wear and the combination of the load sharing by the asperities and the occurrence of chemical reactions constitutes the lubrication regime commonly referred to as the boundary lubrication regime.

Boundary lubrication conditions force the interactions between the two surfaces to take place in the form of asperities colliding with each other and these collisions produce a wide range of consequences at the asperity level, from elastic deformation to plastic deformation to fracture. These collisions produce friction, heat, and sometimes wear. Chemical reactions between lubricant molecules and surfaces usually accompany such collisions producing organic and inorganic surface films and it has long been thought that surface films protect against wear [30].

2.1.1.2 Mixed Lubrication

If the lubricating film which separates the surfaces allows some contact between the deformed asperities, then this type of lubrication is considered as mixed lubrication. In mixed lubrication regime, the contact load is shared between the contacting asperities and the film (Figure 2.3).

In mixed lubrication regime, usually two lubrication mechanisms act simultaneously and both are essential for lowering friction and wear in the contact. In many cases of mixed lubrication regime, most of the applied load is supported by hydrodynamic or EHL lubrication. However, some additional lubrication mechanism is required to reduce friction and wear in contacts between large asperities from opposing surfaces. Even if the fraction of load supported by non-hydrodynamic means is small, severe wear and perhaps seizure can occur if this additional component of lubrication is not available.
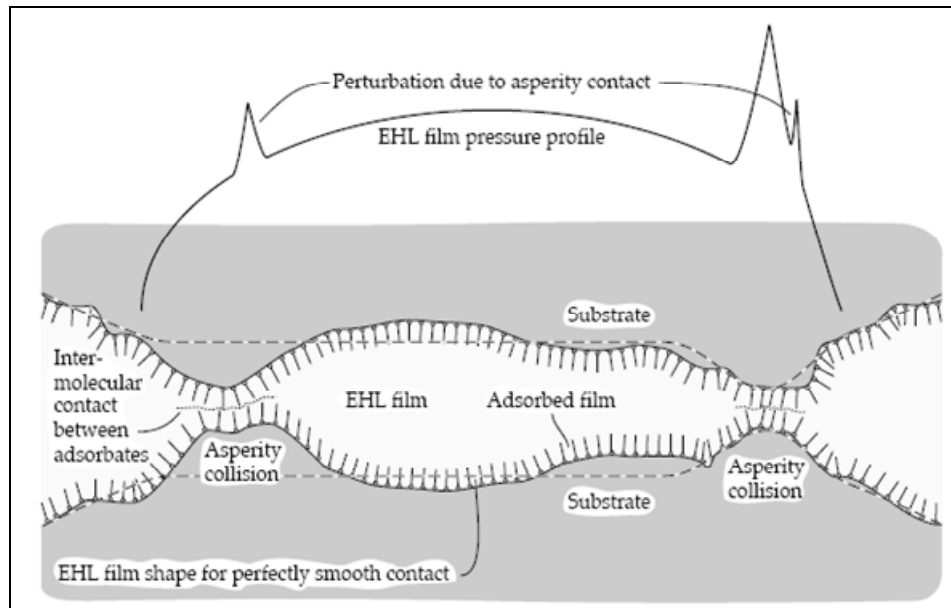
Figure 2.3 Mixed Lubrication Model [31]

Mixed lubrication allows much smaller film thicknesses than pure hydrodynamic lubrication or elastohydrodynamic lubrication. Reduced film thickness coincides with increased load and contact pressure, if other factors remain unchanged, and this characteristic is the basic reason for the importance of mixed lubrication.

Although in most cases when this lubrication regime is active, the collisions between asperities are prevented from inducing any severe forms of wear, a sudden and severe mode of lubrication failure known as scuffing can occur. This can cause serious industrial problems since scuffing can occur precipitately in an apparently well lubricated contact [31].

2.1.1.3 Hydrodynamic Lubrication

In hydrodynamic lubrication regime, the sliding surfaces are separated by a relatively thick film of fluid lubricant and the normal load is supported by the pressure within this film, which is generated hydrodynamically. For hydrodynamic lubrication the opposing surfaces must be so closely matched in dimensions that they are separated by only a small gap over a relatively large area. The gap between the two surfaces is filled with the lubricating fluid which can be oil or grease or, less commonly, water, air, or other liquid or gas.

The pressure which supports the normal load in hydrodynamic lubrication regime, results from viscous forces within the lubricant, which in turn result from the relative motion of the two surfaces. In order to form a hydrodynamic film between sliding

16

surfaces; the gap between them mustn't be parallel and it must converge and also the separations of the surfaces, and the angles of convergence, are typically very small [32].

2.1.1.4 Elastohydrodynamic Lubrication

Elastohydrodynamic lubrication can be defined as a form of hydrodynamic lubrication where the elastic deformation of the contacting bodies and the changes of viscosity with pressure play fundamental roles. In this regime, the influence of elasticity is not limited to second-order changes in load capacity or friction and instead of this; the deformation of the bodies has to be included in the basic model of elastohydrodynamic lubrication. The same also refers to the changes in viscosity due to pressure.

The combination of three effects which are hydrodynamics, elastic deformation of the metal surfaces and the increase in the viscosity of oil under extreme pressures are instrumental to elastohydrodynamic lubrication. At this stage, it should be realized that elastohydrodynamic lubrication is effectively limited to oils as opposed to other viscous liquids because of the pressure-viscosity dependence. It was shown theoretically that under conditions of intense contact stress a lubricating oil film can be formed. The lubricated contacts in which these three effects take place are said to be operating elastohydrodynamically, which effectively means that the contacting surfaces deform elastically under the hydrodynamic pressure generated in the layer of lubricating film. The lubricating films are very thin, but manage to separate the interacting surfaces, resulting in a significant reduction of wear and friction. Although this regime generally operates between nonconforming surfaces, it can also occur under certain circumstances in the contacts classified as conformal such as highly loaded journal and pad bearings which have a significant component of contact and bending deformation. However, enormous loads are required for this to occur and very few journal or pad bearings operate under these conditions [31].

2.1.2 Boundary Conditions

In order to solve the Reynolds equation some boundary conditions are need to be used and in literature there several different boundary conditions which were suggested for the solution of Reynolds equation.

The first one of these boundary conditions is called Full-Sommerfeld boundary condition. This boundary condition is the most obvious and simplest of the boundary conditions and it assumes that the pressures at the trailing and leading edges of the wedge are equal to the outlet and inlet pressures [31]. The boundary condition can be seen on Figure 2.4 and is given as;

$$p = p_1 \qquad at \qquad x = x_1 \tag{2.2}$$

$$p = p_2 \qquad at \qquad x = x_4 \tag{2.3}$$

where;

$p_1 = Inlet\ Pressure \qquad x_1 = Lubrication\ Start\ Point$
$p_2 = Outlet\ Pressure \qquad x_4 = Lubrication\ End\ Point$
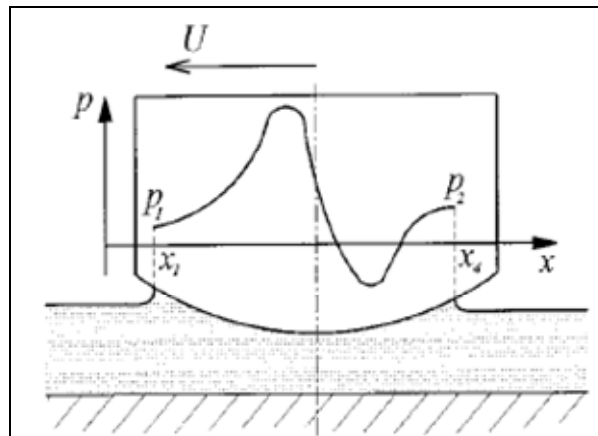
Figure 2.4 Full-Sommerfeld Boundary Condition [33]

It can be seen that the Full-Sommerfeld boundary condition is unlikely to apply to real fluids. There is a large negative pressure in the diverging region which is the mirror image of the pressure distribution in the converging region. As it is known, large negative pressures are physically unrealistic. Furthermore, because of these opposing negative and positive pressures the predicted load capacity is lower than the real one. On the other hand, it has been shown that the hydrodynamic lubrication film is very efficient under such geometries and is capable of supporting a load. Hence some other boundary condition should apply.

The second of these boundary conditions is called Half-Sommerfeld boundary condition and it is the modified version of Full-Sommerfeld boundary condition in order to eliminate the negative pressures at the diverging section because of the

limitations of the lubricants. According to this boundary condition the negative pressures which are predicted according to Full-Sommerfeld boundary condition are simply neglected and set to zero gauge or atmospheric absolute pressure [31].

From the engineering view point the Half-Sommerfeld boundary condition is very simple and easy to apply. However its physical basis is erroneous since discontinuity of flow at the boundary between the zero and non-zero pressure regions is implied.

The third of these boundary conditions is called Reynolds boundary condition. In this boundary condition there are no negative pressures and the conditions at the boundaries of the lubricated zone are given as (Figure 2.5);

$$p = p_1 \qquad\qquad at \qquad x = x_1 \qquad\qquad\qquad (2.4)$$

$$p = p_2 \quad \& \quad \frac{dp}{dx} = 0 \qquad at \qquad x = x_2 \qquad\qquad\qquad (2.5)$$

where;

$p_1 = Inlet\ Pressure$ $\qquad\qquad x_1 = Lubrication\ Start\ Point$
$p_2 = Outlet\ Pressure$ $\qquad\qquad x_2 = Film\ Rupture\ Point$
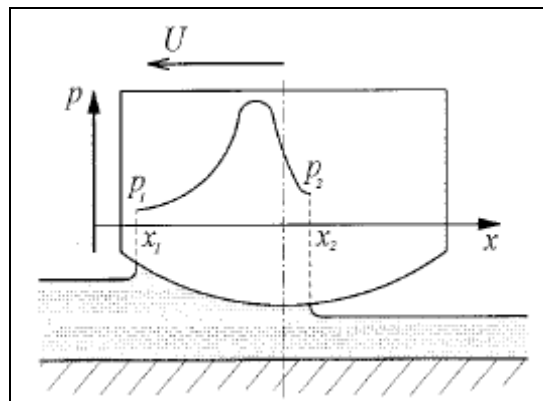
Figure 2.5 Reynolds Boundary Condition [33]

Reynolds boundary condition is superior to the half-Sommerfeld condition since it correctly accounts for oil flow continuity across the cavitation boundary [33].

Moreover another boundary condition which is similar to Reynolds boundary condition is also exists. Its difference from Reynolds boundary condition is that a film reformation is also allowed. This boundary condition is formulated by Dowson et al. and the conditions at the lubricated zone are given as (Figure 2.6);

$$p = p_1 \qquad\qquad at \qquad\qquad x = x_1 \qquad\qquad (2.6)$$

$$p = 0 \quad \& \quad \frac{dp}{dx} = 0 \qquad\qquad at \qquad\qquad x = x_2 \qquad\qquad (2.7)$$

$$p = 0 \quad \& \quad \frac{dp}{dx} = 6\eta U \left(\frac{h_3 - h_2}{h_3^3} \right) \qquad at \qquad\qquad x = x_3 \qquad\qquad (2.8)$$

$$p = p_2 \qquad\qquad at \qquad\qquad x = x_4 \qquad\qquad (2.9)$$

where;

$p_1 = Inlet\,Pressure$ $\qquad\qquad p_2 = Outlet\,Pressure$

$x_1 = Lubrication\,Start\,Point$ $\quad x_2 = Film\,Rupture\,Point$

$x_3 = Film\,Reformation\,Point$ $\quad x_4 = Lubrication\,End\,Point$
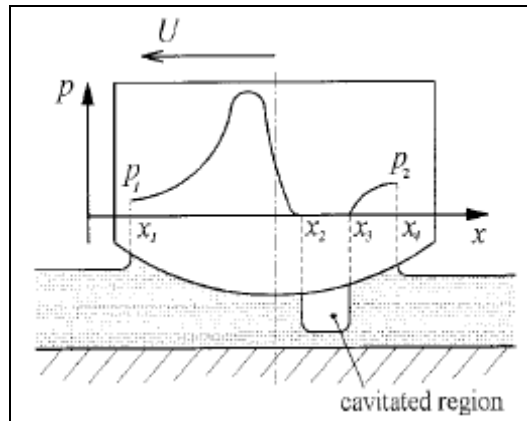
Figure 2.6 Reynolds Boundary Condition with Film Reformation [33]

As the last boundary condition which is suggested by Dowson and Taylor, it is considered that the flow separation occurs rather than cavitation. The simplest flow separation condition which is referred to as the full fluid condition may be derived from the Navier-Stokes equation. In the piston ring cylinder wall interface the piston ring is considered to be the stationary surface in terms of the hydrodynamic model and lubricant entrainment. Hence, the flow separates from the piston ring at the outlet gas pressure and the pressure gradient condition is derived from the Navier-Stokes equation at the outlet region. The conditions for this boundary condition suggestion are (Figure 2.7);

$$p = p_1 \qquad\qquad at \qquad x = x_1 \qquad\qquad (2.10)$$

$$p = p_2 \quad \& \quad \frac{dp}{dx} = \frac{2\eta U}{h_2^2} \qquad\qquad at \qquad x = x_2 \qquad\qquad (2.11)$$

where;

$p_1 = Inlet\ Pressure$ $\qquad\qquad$ $x_1 = Lubrication\ Start\ Point$

$p_2 = Outlet\ Pressure$ $\qquad\qquad$ $x_2 = Lubrication\ End\ Point$
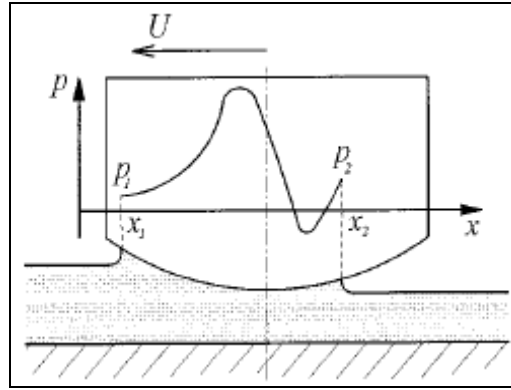
Figure 2.7 Flow Separation Boundary Condition [33]

However, the full fluid film condition is only approximate, since a full fluid film is assumed and no development of the lubricant/gas interface is considered. In order to overcome this deficiency Coyne and Elrod developed a two-dimensional Newtonian analysis that defines the shape of the lubricant-gas interface and includes the effects of gravity, inertia and surface tension. That's why in piston ring lubrication, gravity and inertia effects are negligible the pressure and pressure gradient at the point of separation are given as;

$$p = p_1 \qquad\qquad\qquad at \qquad x = x_1 \qquad\qquad (2.12)$$

$$p = p_2 \quad \& \quad \frac{dp}{dx} = \frac{6\eta U}{h_2^2}\left(1 - 2\frac{h_\infty}{h_2}\right) \qquad at \qquad x = x_2 \qquad\qquad (2.13)$$

where;

$p_1 = Inlet\ Pressure$ $\qquad\qquad$ $x_1 = Lubrication\ Start\ Point$

$p_2 = Outlet\ Pressure$ $\qquad\qquad$ $x_2 = Lubrication\ End\ Point$

In this revised condition h_∞ is the asymptotic film thickness downstream of the separation point.

2.1.3 Cavitation and Film Rupture

Cavitation and rupture are two main ways of film separation between two surfaces in the fluid flow. The phenomenon of cavitation in fluids occurs when the local fluid pressure falls below atmospheric pressure. The reason for this is that most liquids contain dissolved air and minute dirt particles. In cavitation phenomenon, the formation of a cavity or cavities of gas or vapour within the body of the fluid occurs because of the inability of the lubricant to sustain large and continuous negative pressures [31]. The formation of cavities and their subsequent development affects the pressure generated in the continuous thin lubricant film and, thus, any integrated quantities such as the load capacity. In general, there are two forms of cavitation [34]:

a) Gaseous Cavitation: In this type of cavitation gas cavities may arise in a lubricant film whenever subambient pressures occur.

b) Vaporous Cavitation: This type of cavitation develops where the pressure in a lubricant film falls to its vapour pressure, giving rise to boiling of the lubricant at local ambient temperature.

The critical difference between gaseous cavitation, and vaporous cavitation is that in vaporous cavitation there are bubbles of dissolved air in vaporous cavitation and sudden bubble collapse is also possible. When a bubble collapses against a solid surface very high stresses are generated and this will usually cause wear [31].

The occurrence of gaseous cavitation may be a natural consequence with a convergent–divergent geometry in the liquid film like in reciprocating piston rings. The mechanisms responsible for cavitation are [34]:

a) lubricant flow through a converging–diverging wedge,

b) reverse squeezing in bearings, when the journal surface moves away rapidly from the bearing wall,

c) shear-thinning of the fluid by varying film thickness,

d) reciprocating speed, varying load and temperature, leading to variable film thickness.

The reciprocating motion of the piston rings causes superambient pressures at the converging wedge and subambient or negative pressures at the diverging wedge and

because of this a film breakdown occurs in two different ways. The first film breakdown depends on the balance between viscous shear and surface tension forces and the second one is due to vaporous cavitation, which may occur if the first rupture allows the formation of sufficiently low pressures.

As it is shown in Figure 2.8 there are three types of cavities. The first one which is called fern shaped cavity occurs at the inside of the lubrication zone and it is a closed cavitation. In this type of cavities a film reformation occurs at the traling edge of the piston ring. In the second type of cavity string shaped cavities are formed and these are the combined form of fern shaped cavities. This one is also a closed cavitation and a film reformation is valid for them. For the last cavity type which is an open cavitation, no film reformation occurs at the trailing edge of the ring and Reynolds boundary condition allows this kind of cavities which doesn't allow film reformation.
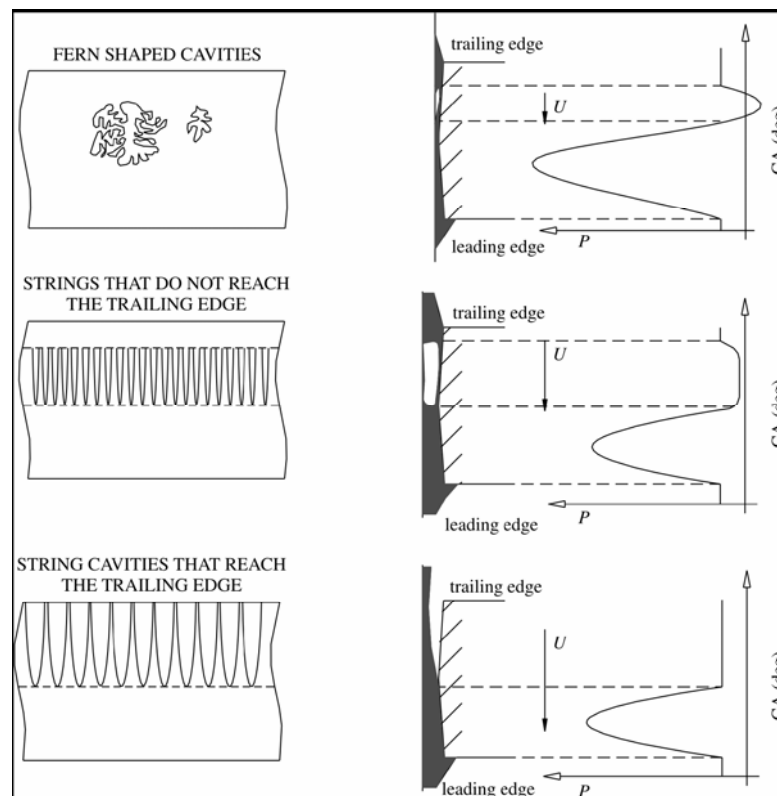
Figure 2.8 Cavity Types and Corresponding Pressure Profiles [34]

2.2 Governing Equations for Ring Dynamics

In this part of the study the main equations which are used to solve the problem were told.

23

2.2.1 Forces Acting on a Piston Ring

There are several forces acting on a piston ring and these forces are shown in Figure 2.9.
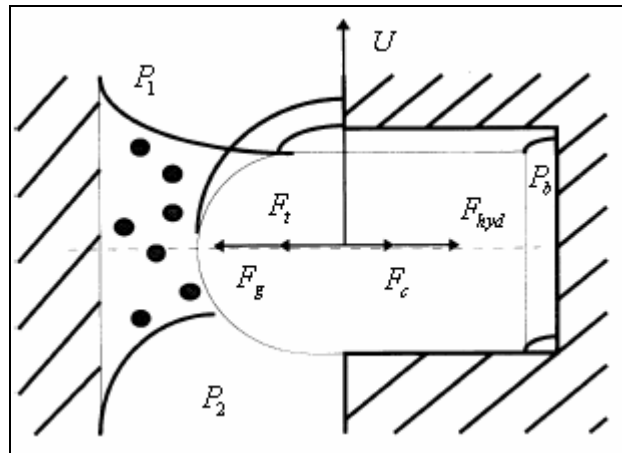
Figure 2.9 Forces and Pressures Acting on the Piston Ring [6]

As it can be seen from Figure 2.9 forces acting on a piston ring are being formed because of the pressures which are effective on the ring. These forces and pressures are;

p_1 = Inlet Pressure

p_2 = Outlet Pressure

p_b = Back Pressure

F_t = Ring Tension Force

F_g = Gas Force which is a result of Back Pressure

F_{hyd} = Hydrodynamic Force

F_c = Asperity Contact Force

2.2.2 Reynolds Equation

The distribution of pressure within a hydrodynamic lubricant film is described by the Reynolds equation, which is derived from the Navier-Stokes equations for fluid flow by assuming that the flow is laminar, that the fluid film is thin compared with its other dimensions and that the dominant forces are due to viscosity. This equation is given as;

24

$$\frac{\delta}{\delta x}\left(\frac{h_T^3}{12\mu}\frac{\delta p}{\delta x}\right)+\frac{\delta}{\delta x}\left(\frac{h_T^3}{12\mu}\frac{\delta p}{\delta y}\right)=\frac{U_1+U_2}{2}\frac{\delta h_T}{\delta x}+\frac{\delta h_T}{\delta t} \qquad (2.14)$$

where x is the sliding direction, U_1 and U_2 are the velocities of the sliding surfaces and h_T is the mean local film thickness.

In Reynolds equation the terms which are on the left hand side denote the mass transports in x and y directions. The first term on the right hand side is the mass transport due to film thickness change along the flow direction and last term at the right hand side denotes the squeeze film effect which is about the change of film thickness with the motion of the surfaces towards each other.

Patir and Cheng [35] modified the Reynolds Equation in order to include surface roughness effects on partially lubricated contacts. This modified Reynolds equation is called Average Reynolds equation and expressed as;

$$\frac{\delta}{\delta x}\left(\phi_x\frac{h^3}{12\mu}\frac{\delta \overline{p}}{\delta x}\right)+\frac{\delta}{\delta y}\left(\phi_y\frac{h^3}{12\mu}\frac{\delta \overline{p}}{\delta y}\right)=\frac{U_1+U_2}{2}\frac{\delta h_T}{\delta x}+\frac{U_1-U_2}{2}\sigma\frac{\delta \phi_s}{\delta x}+\frac{\delta \overline{h_T}}{\delta t} \qquad (2.15)$$

where ϕ_x and ϕ_y are pressure flow factors and ϕ_s is the shear flow factor. These parameters are given by Patir and Cheng and they are the functions of surface roughness characteristics.

2.2.3 Flow Factors

As it is told before Patir and Cheng modified the Reynolds equation and derived the Average Reynolds equation by using pressure and shear flow factors. Pressure flow factors which are ϕ_x and ϕ_y compare the average pressure flow in a rough surface to that of a smooth one. The parameter ϕ_s which is the shear flow factor represents the additional flow transport due to sliding in a rough surface. These parameters are given as a function of H_σ and γ and expressed as [35, 36];

$$\phi_x = \phi_x\left(H_\sigma,\gamma\right) \qquad (2.16)$$

$$\phi_y = \phi_y\left(H_\sigma,\gamma\right) \qquad (2.17)$$

$$\phi_s = \phi_s\left(H_\sigma,\gamma\right) \qquad (2.18)$$

where H_σ is the ratio of local film thickness to composite surface roughness and γ is the Peklenik factor which shows the orientation of the surface roughness. H_σ is expressed as;

$$H_\sigma = \frac{h}{\sigma} \tag{2.19}$$

and the composite surface roughness σ is calculated as;

$$\sigma = \sqrt{\sigma_1^2 + \sigma_2^2} \tag{2.20}$$

Peklenik factor is defined as;

$$\gamma = \frac{\lambda_{o.5x}}{\lambda_{0.5y}} \tag{2.21}$$

where $\lambda_{0.5x}$ and $\lambda_{0.5y}$ are the lengths at which auto-correlation of a profile reduces to 50 percent of its initial value in the longitudinal and transversal directions respectively (Figure 2.10).
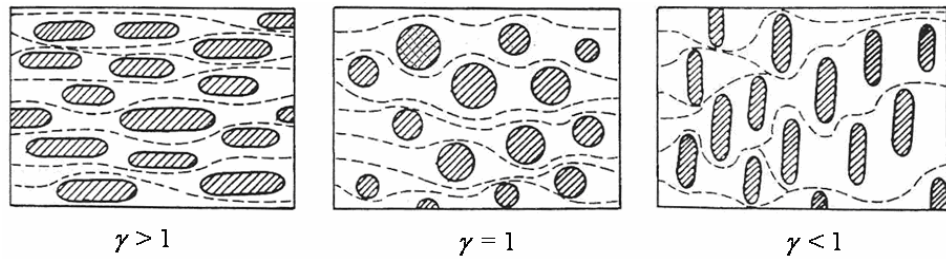
Figure 2.10 Peklenik Factor [35]

The change of pressure flow factor φ_x with H_σ is shown in Figure 2.11. For every different value of Peklenik factor, pressure flow factor φ_x is given as different curves as seen on Figure 2.11 and it can be calculated with;

$$\phi_x = \begin{cases} 1 - Ce^{-rH_\sigma} & \gamma \le 1 \\ 1 + CH_\sigma^{-r} & \gamma > 1 \end{cases} \tag{2.22}$$
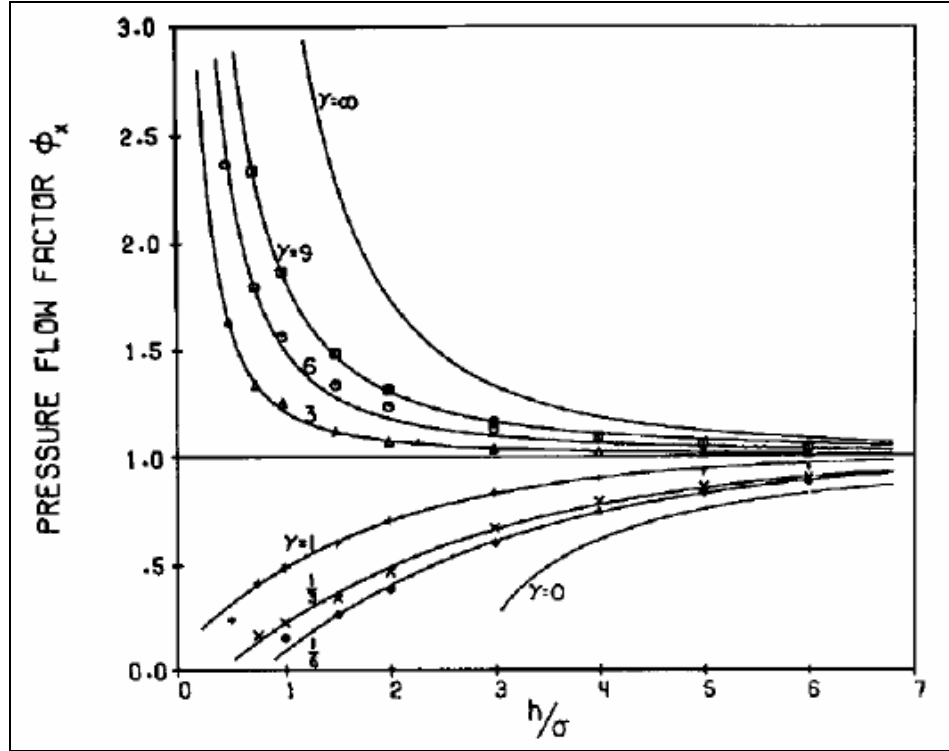
Figure 2.11 Pressure Flow Factor [35]

For a surface roughness with a given γ value, φ_y is equal to the φ_x value corresponding to $1/\gamma$ at it can be found as;

$$\phi_y\left(H_\sigma,\gamma\right)=\phi_x\left(H_\sigma,\frac{1}{\gamma}\right) \tag{2.23}$$

The parameters C and r for pressure flow factor formulas are given in Table C.1.

Shear flow factor φ_s (Figure 2.12) is a function of H_σ, the standard deviations σ_1 and σ_2, and the Peklenik factor values γ_1 and γ_2 of the two opposing surfaces. Dependence of shear flow factor to these parameters is given as;

$$\phi_s=V_{r1}\Phi_s\left(H_\sigma,\gamma_1\right)-V_{r2}\Phi_s\left(H_\sigma,\gamma_2\right) \tag{2.24}$$

where V_{r1} and V_{r2} are the variance ratios given by;

$$V_{r1}=\left(\frac{\sigma_1}{\sigma}\right)^2 \tag{2.25}$$

$$V_{r2}=\left(\frac{\sigma_2}{\sigma}\right)^2 \tag{2.26}$$

27
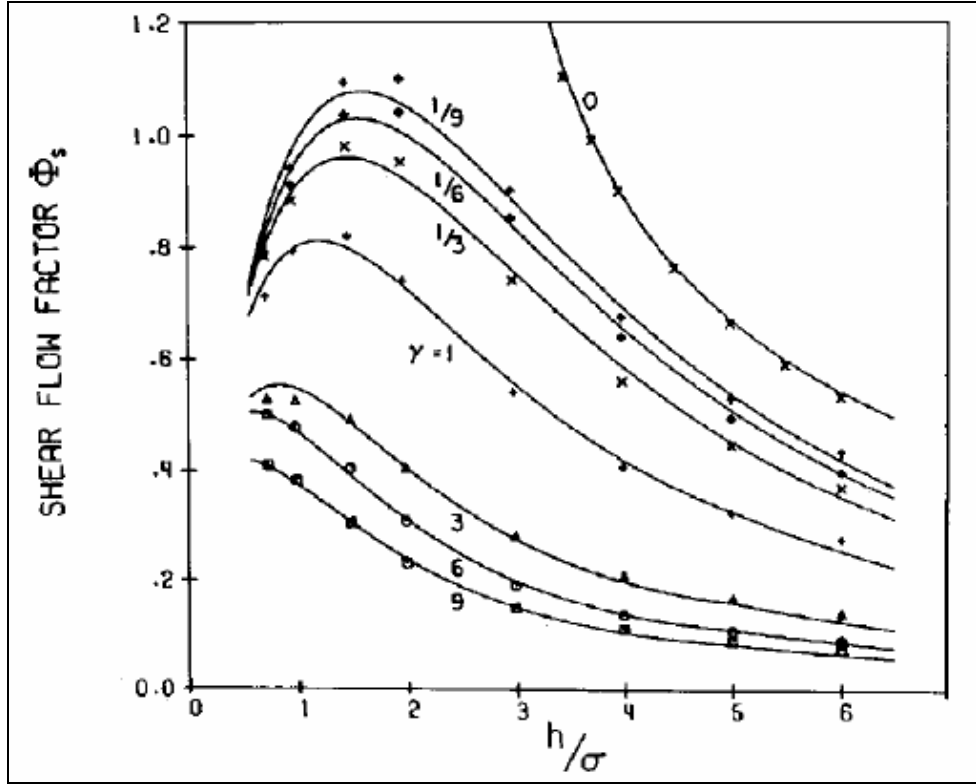
Figure 2.12 Shear Flow Factor [36]

Φ_s in Eq. (2.24) is also called shear flow factor but it is associated with a single surface, while φ_s is associated with the combination of two surfaces and it is expressed as;

$$\Phi_s = \begin{cases} A_1 H_\sigma^{\alpha_1} e^{-\alpha_2 H_\sigma + \alpha_3 H_\sigma^2} & H_\sigma \le 5 \\ A_2 e^{-0.25 H_\sigma} & H_\sigma > 5 \end{cases} \tag{2.27}$$

The parameters for the calculation of Φ_s are given at the Table C.2.

2.2.4 Asperity Contact Force

According to Greenwood and Tripp's asperity contact model [37], the average contact pressure is given with;

$$p_c = K'E'F_{2.5}(H_\sigma) \tag{2.28}$$

where;

$$K' = \frac{8\sqrt{2}}{15} \pi (N\beta'\sigma) \sqrt{\frac{\sigma}{\beta'}} \tag{2.29}$$

And composite Young's modulus;

$$E' = \frac{2}{\left(\dfrac{1-\upsilon_1^2}{E_1} + \dfrac{1-\upsilon_2^2}{E_2} \right)} \tag{2.30}$$

In Eq. (2.29) N is the number of asperities per unit contact area, β' is the asperity radius of curvature and σ is the variance of the composite surface roughness. The function $F_{2.5}(H_\sigma)$ is the probability distribution of asperity heights. This function is simplified by Hu et al. [38] and given as;

$$F_{2.5}\left(H_\sigma\right) = \begin{cases} A\left(\Omega - H_\sigma\right)^Z & H_\sigma \leq \Omega \\ 0 & H_\sigma > \Omega \end{cases} \tag{2.31}$$

where the parameters in Eq. (2.29) and Eq. (2.31) which are given by Hu et al. are;

$\Omega = 4.0$

$A = 4.4068 \times 10^{-5}$

$Z = 6.804$

$K' = 1.198 \times 10^{-4}$

3 SOLUTION APPROACH

In this study, a MATLAB code was written in order to investigate the effect of LST on the tribological performance of a piston ring – cylinder bore pair and in this part the solution approach will be explained.

3.1 Assumptions

In order to solve the problem several assumptions were done and the code was generated in the light of these assumptions.

3.1.1 Flow and Lubricant Properties

As it was explained in theory section, the flow is assumed to be isoviscous, laminar and thought to take place in an almost parallel thin film of negligible curvature.

For the lubricant properties, it is assumed to be an incompressible and Newtonian fluid and its viscosity is also assumed to be constant and there is no change at viscosity because of the deviation of the temperature and pressure over whole engine cycle.

3.1.2 Inlet Oil Supply

In this study, partially flooded inlet condition is used. According to this inlet condition it is assumed that there is always a lubricant film at the inlet of the ring which has a constant thickness h_{max}. But the lateral motion of piston ring in the groove changes the lubrication start point at the converging section and because of this; constant film thickness matches with a different point of the ring for every crankangle.

3.1.3 Surface Properties

In micro scale the surfaces of piston ring and cylinder bore were thought to be rough and it is assumed that the roughness heights have a Gaussian frequency density for both surfaces. However in macro scale, there are dimples with a given depth on the

liner surface and the distribution of the dimples can be determined in order to optimize the tribological performance of the system.

3.1.4 Structural Properties

In this study, cylinder bore was thought to be perfect cylindrical and the ring is thought to be axi-symmetrical and there is no distortion on both ring and bore. Because of this assumption, the nominal film thickness, which is the film thickness at the peak of the ring profile, doesn't change in peripheral direction. Also, it is assumed that, piston ring doesn't make any twist or tilt motion and it can only move up and down in its groove.

3.2 Solution of Reynolds Equation

Since, the Reynolds equation is a second order non-linear differential equation, finite differencing method is used to solve the equation. In the case of piston ring - cylinder bore interaction, cylinder bore is stationary and therefore $U_1 = 0$ and $U_2 = U$, so Eq. (2.15) can be written as;

$$\frac{\delta}{\delta x}\left(\phi_x h^3 \frac{\delta \overline{p}}{\delta x}\right) + \frac{\delta}{\delta y}\left(\phi_y h^3 \frac{\delta \overline{p}}{\delta y}\right) = 6\mu U\left(\frac{\delta h_T}{\delta x} + \sigma \frac{\delta \phi_s}{\delta x}\right) + 12\mu \frac{\delta \overline{h_T}}{\delta t} \tag{3.1}$$

Before applying finite differencing method, "Average Reynolds" equation is normalized by using some non-dimensional parameters. These non-dimensional parameters are;

$$X = \frac{2x}{b} \tag{3.2}$$

$$Y = \frac{2y}{b} \tag{3.3}$$

$$U^* = \frac{U}{r\omega} \tag{3.4}$$

$$T = t\omega \tag{3.5}$$

$$\sigma^* = \frac{\sigma}{c} \tag{3.6}$$

$$\phi_c = \frac{\partial \overline{h_t}}{\partial h} \tag{3.7}$$

$$P = \overline{p} \frac{c^2}{3\mu r \omega b} \tag{3.8}$$

where ϕ_c is the contact factor which is defined by Wu and Zheng [39] in order to simplify the calculation of the average gap between the surfaces and it is defined with the error function and given as;

$$\phi_c = \frac{1}{2}\left(1 + erf\left(H_\sigma\right)\right) \tag{3.9}$$

In this way, non-dimensional form of Average Reynolds equation takes the form of;

$$\frac{\delta}{\delta X}\left(\phi_x H^3 \frac{\delta P}{\delta X}\right) + \frac{\delta}{\delta Y}\left(\phi_y H^3 \frac{\delta P}{\delta Y}\right) = U^*\left(\phi_c \frac{\delta H}{\delta X} + \sigma^* \frac{\delta \phi_s}{\delta X}\right) + \beta \phi_c \frac{\delta H}{\delta T} \tag{3.10}$$

where β is the squeeze film factor. In Eq. (3.10) ϕ_x, ϕ_y, ϕ_s, ϕ_c, H and P are all the functions of X and Y and because of this they will be solved numerically. Non-dimensional Average Reynolds equation can also be written in the form of;

$$\begin{aligned}
\left(H^3 \frac{\delta P}{\delta X}\frac{\delta \phi_x}{\delta X} + 3H^2\phi_x \frac{\delta H}{\delta X}\frac{\delta P}{\delta X} + \phi_x H^3 \frac{\partial^2 P}{\partial X^2}\right) \\
+ \left(H^3 \frac{\delta P}{\delta Y}\frac{\delta \phi_y}{\delta Y} + 3H^2\phi_y \frac{\delta H}{\delta Y}\frac{\delta P}{\delta Y} + \phi_y H^3 \frac{\partial^2 P}{\partial Y^2}\right) \\
= U^*\left(\phi_c \frac{\delta H}{\delta X} + \sigma^* \frac{\delta \phi_s}{\delta X}\right) + \beta \phi_c \frac{\delta H}{\delta T}
\end{aligned} \tag{3.11}$$

3.3 Mesh Formation

As it was explained, finite differencing method was used to solve the non-dimensional Average Reynolds equation. According to finite differencing method first and second derivatives of any property like Ω in X and Y directions can be expressed as;

$$\frac{\delta \Omega}{\delta X} = \frac{\Omega_{i+1,j} - \Omega_{i-1,j}}{2\Delta X} \tag{3.12}$$

$$\frac{\delta\Omega}{\delta Y} = \frac{\Omega_{i,j+1} - \Omega_{i,j-1}}{2\Delta Y} \tag{3.13}$$

$$\frac{\partial^2\Omega}{\partial X^2} = \frac{\Omega_{i+1,j} - 2\Omega_{i,j} + \Omega_{i-1,j}}{(\Delta X)^2} \tag{3.14}$$

$$\frac{\partial^2\Omega}{\partial Y^2} = \frac{\Omega_{i,j+1} - 2\Omega_{i,j} + \Omega_{i,j-1}}{(\Delta Y)^2} \tag{3.15}$$

Eq.s (3.12-15) can be applied on a meshed surface like in Figure 3.1 and the first and second derivatives at the center node can be taken.
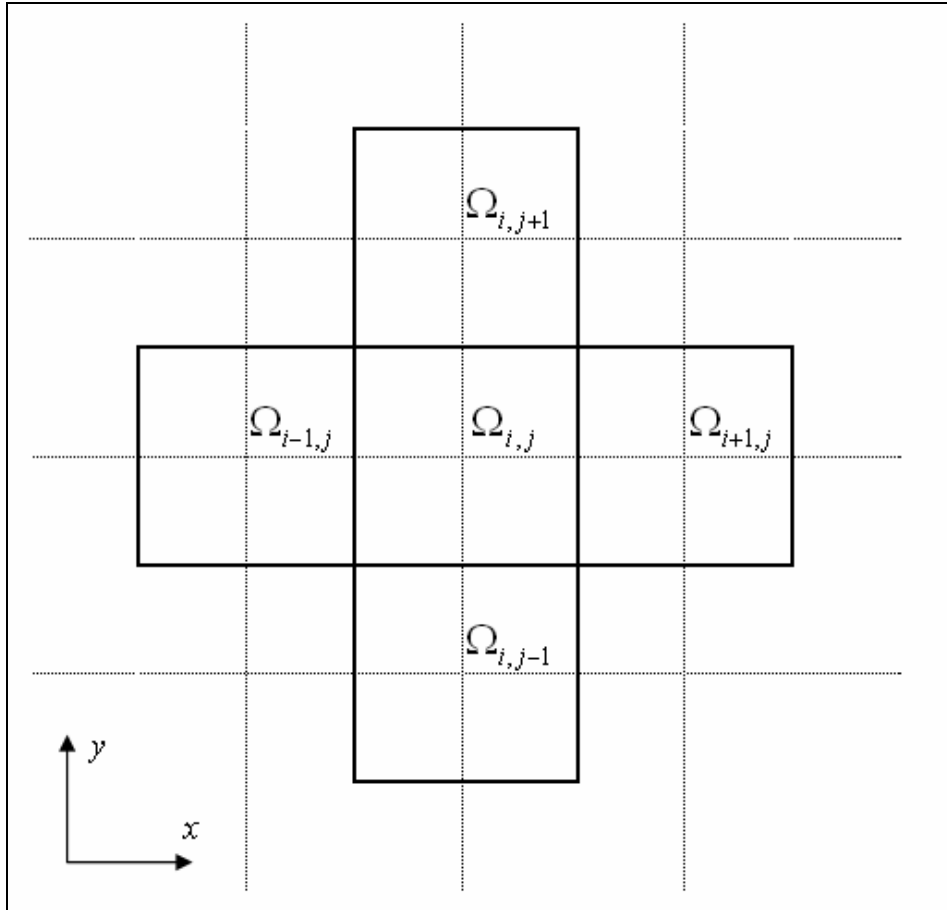
Figure 3.1 Mesh Formation for Finite Differencing Method

Applying the derivation formulas for finite differencing method to the non-dimensional Average Reynolds equation, the discretized form of this equation can be obtained as;

$$P_{i+1,j}C_{i+1,j} + P_{i-1,j}C_{i-1,j} + P_{i,j}C_{i,j} + P_{i,j+1}C_{i,j+1} + P_{i,j-1}C_{i,j-1} = S_{i,j} \tag{3.16}$$

where $P_{i+1,j}$, $P_{i-1,j}$, $P_{i,j+1}$ and $P_{i,j-1}$ are the hydrodynamic pressure values for the adjacent nodes, $C_{i+1,j}$, $C_{i-1,j}$, $C_{i,j+1}$ and $C_{i,j-1}$ are the constants for these nodes and $S_{i,j}$ is the right hand side of the discretized equation. The constants and the right hand side of the equation can be given as;

$$C_{i+1,j} = \left\{ \frac{H_{i,j}^2}{4\Delta X^2} \left[H_{i,j} \left(\phi_{x_{i+1,j}} + 4\phi_{x_{i,j}} - \phi_{x_{i-1,j}} \right) + 3\phi_{x_{i,j}} \left(H_{i+1,j} - H_{i-1,j} \right) \right] \right\} \tag{3.17}$$

$$C_{i-1,j} = \left\{ \frac{H_{i,j}^2}{4\Delta X^2} \left[H_{i,j} \left(-\phi_{x_{i+1,j}} + 4\phi_{x_{i,j}} + \phi_{x_{i-1,j}} \right) + 3\phi_{x_{i,j}} \left(-H_{i+1,j} + H_{i-1,j} \right) \right] \right\} \tag{3.18}$$

$$C_{i,j} = \left\{ -2H_{i,j}^3 \left[\frac{\phi_{x_{i,j}}}{\Delta X^2} + \frac{\phi_{y_{i,j}}}{\Delta Y^2} \right] \right\} \tag{3.19}$$

$$C_{i,j+1} = \left\{ \frac{H_{i,j}^2}{4\Delta Y^2} \left[H_{i,j} \left(\phi_{y_{i,j+1}} + 4\phi_{y_{i,j}} - \phi_{y_{i,j-1}} \right) + 3\phi_{y_{i,j}} \left(H_{i,j+1} - H_{i,j-1} \right) \right] \right\} \tag{3.20}$$

$$C_{i,j-1} = \left\{ \frac{H_{i,j}^2}{4\Delta Y^2} \left[H_{i,j} \left(-\phi_{y_{i,j+1}} + 4\phi_{y_{i,j}} + \phi_{y_{i,j-1}} \right) + 3\phi_{y_{i,j}} \left(-H_{i,j+1} + H_{i,j-1} \right) \right] \right\} \tag{3.21}$$

$$S_{i,j} = U^* \left\{ \phi_c \frac{H_{i+1,j} - H_{i-1,j}}{2\Delta X} + \sigma^* \frac{\phi_{s_{i+1,j}} - \phi_{s_{i-1,j}}}{2\Delta X} \right\} + \left\{ \beta\phi_{c_{i,j}} \frac{H^T - H^{T-\Delta T}}{2\Delta T} \right\} \tag{3.22}$$

The general mesh of the piston ring is shown in Appendix A.

3.4 Dimple Formation

In the name of laser surface texturing, geometrically different dimples were created to investigate the tribological performance of the laser surface textured cylinder bores and for the piston ring and cylinder bore interface these dimples were used to calculate the film thickness values. In Figure 3.2, two different shaped dimples can be seen.
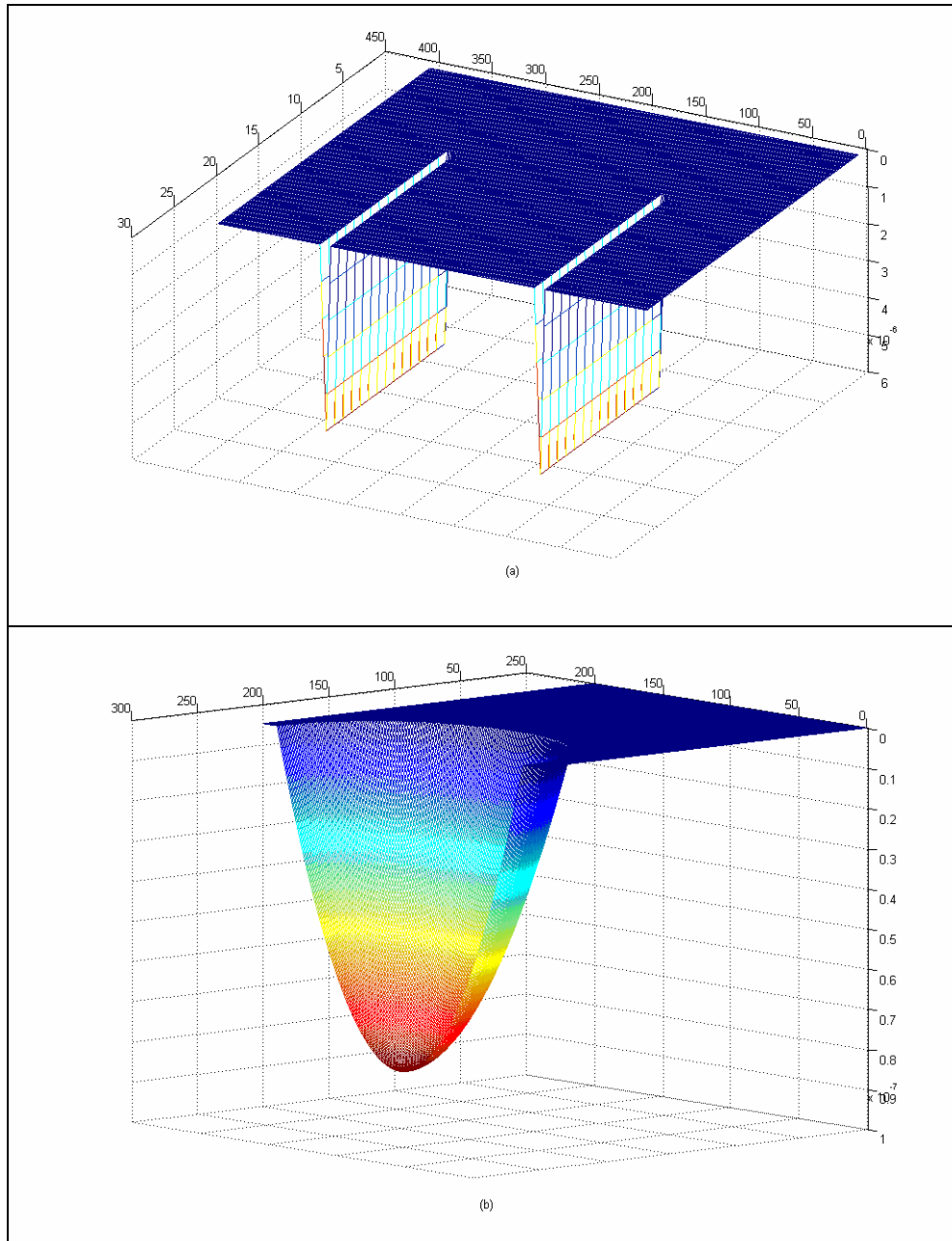
Figure 3.2 Different Shaped Dimple Surfaces (a) Triangular Dimple (b) Spherical Dimple

In this study the dimples were thought to be on the cylinder bore and because of the reciprocating ring motion, a moving cylinder bore is created and dimple profile is calculated for every crankangle.

3.5 Film Thickness Calculation

Film thickness calculation is done with Eq. (3.23) as;

$$h_T = h + h_{dimple} + \delta_1 + \delta_2 \tag{3.23}$$

where h_T is the total film thickness, h is the nominal film thickness, δ_1 and δ_2 are the surface roughness profiles (Figure 3.3). In order to add the dimple effects h_{dimple} is also used in this equation which shows the deviation of film thickness because of the dimple profile.
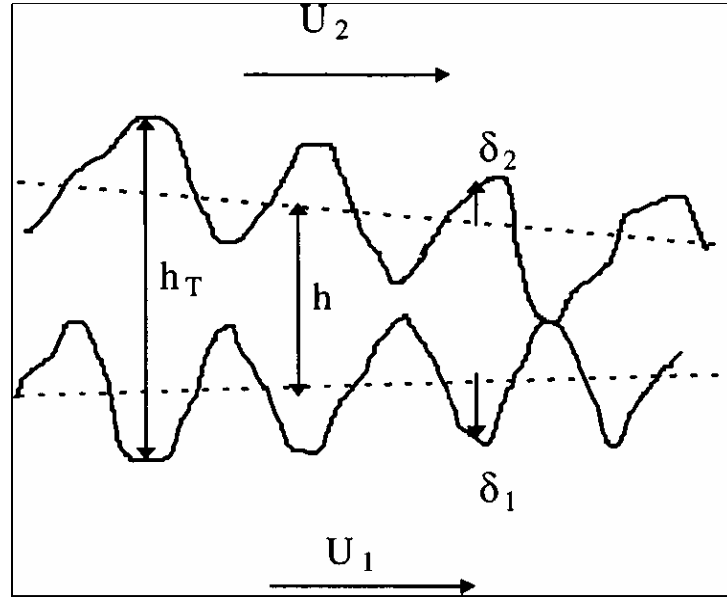
Figure 3.3 Film Thickness

3.6 Solution of Rupture Nodes

Solution of rupture nodes was done according to Reynolds boundary condition which was explained in the theory section of this thesis. According to Reynolds boundary condition the pressure at the rupture zone of the lubricant film must be equal to the outlet pressure and the pressure profile gradient at the rupture zone must be zero.

$$P_{x_2} = P_2 \qquad \& \qquad \frac{\delta P}{\delta x} = 0 \quad at \quad x = x_2 \tag{3.24}$$

where P_2 is the outlet pressure and x_2 is the rupture node. However, in this study some other conditions were added in order to restrict closed cavitations at the dimple area, because cavitation may occur at the diverging section of the dimple which locates inside of the lubrication zone. These conditions aimed not to allow pressures at the wetted zone which are lower than the inlet or outlet pressures. Thus, even the Reynolds boundary condition is satisfied, if there are hydrodynamic pressures which are lower than inlet or outlet pressures in the wetted zone, that rupture node is not accepted as the correct one.

In Figure 3.4 rupture node determination is shown and as it can be seen the cavitation check is started from the last node and it goes backwards until the conditions are satisfied.
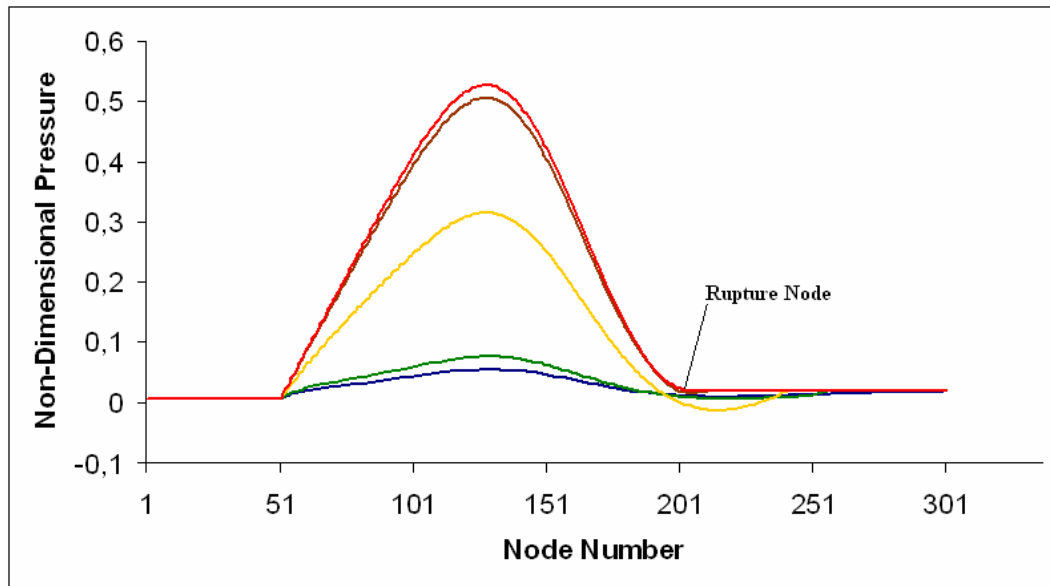
Figure 3.4 Rupture Node Determination

3.7 Force Equilibrium

As it was shown in Figure 2.9, there are four different forces acting on the piston ring in radial direction which are hydrodynamic force, asperity contact force, ring tension force and gas force. In this model friction force and the pressure acting on the sides of the piston ring is neglected. The first and second ones, which are hydrodynamic force and asperity contact force, are the results of the hydrodynamic pressure and asperity contact pressure. These forces are calculated by integrating the hydrodynamic pressure and asperity contact pressure over the lubricated zone. Ring tension force is thought to be a constant force which is given at the design stage of the ring. For the last force, which is the gas force, is a result of the pressure that acts from the back of the piston ring. For this pressure it is thought that ring moves towards the lower pressure side in the piston groove and the higher one of the gas pressure at the inlet or outlet acts from the back of the ring. As shown in Figure 3.5, piston ring moves downwards in the piston groove because of the higher pressure at the upper land.
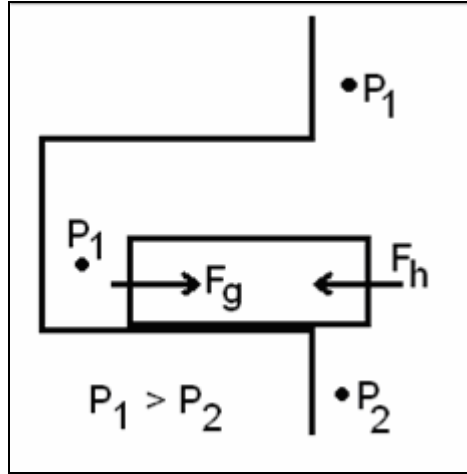
Figure 3.5 Back Pressure Determination [40]

For the force equilibrium condition the total net force acting on the piston ring is calculated with the summation of all radial forces as;

$$F_{total} = F_{hyd} + F_c + F_g + F_t \qquad (3.25)$$

and in order to satisfy the force equilibrium, total force needs to be zero.

$$\sum F_{total} = 0 \qquad (3.26)$$

3.8 Code Description

This code was prepared in order to solve the dynamics of a piston ring which reciprocates on a laser textured cylinder bore over a whole engine cycle and an iterative solution technique is used. As it was explained before to add the effects of surface roughness Average Reynolds equation was used instead of Reynolds equation, which was modified by Patir and Cheng. Also an asperity contact model was added to the model in order to solve the problem for both mixed and hydrodynamic lubrication regimes. Since the cylinder was a laser textured one; a floating cylinder bore model was used. By the help of the floating cylinder bore model, bore section profile which is in front of the piston ring is calculated by using the ring reciprocating motion and as a result of this; problem was solved for each crankangle for different cylinder bore – piston ring interface. The flowchart of the code is given in Appendix B.

4 RESULTS AND DISCUSSION

4.1 Global Data of the Engine

The engine which is modeled for this study was Ford-Otosan Ecotorque 9L heavy duty diesel engine and general data for this engine is given at Table 4.1.

Table 4.1 Global Data of the Engine

Engine Configuration	6 Cylinder in-line
Fuel Injection System	Common Rail DI Diesel (1800 bar)
Scavenging System	Turbo-Charged, Inter-Cooled
Bore	115 mm
Stroke	144 mm
Swept Volume	8.974 L
Peak firing pressure	190 bar
Rated power	295 kW @ 2200 rpm
Peak torque	1600 Nm @ 1200 rpm
Max. Operational Speed	2200 rpm
Max. Continuous Over Speed	3100 rpm
Valve Train	OHV (Overhead Valve), 4 valves per cylinder

The analyses were done under 50% loads and at 1680 rpm.

4.2 Lubricant Film Thickness

4.2.1 Conventional Cylinder Bore Results

According to the program results first of all it can be seen that the program gives the expected results for conventional cylinder bores. In Figure 4.1 the film thickness are shown. As it is seen through Figure 4.1 minimum film thickness is obtained after the FTDC which is 360 CA.
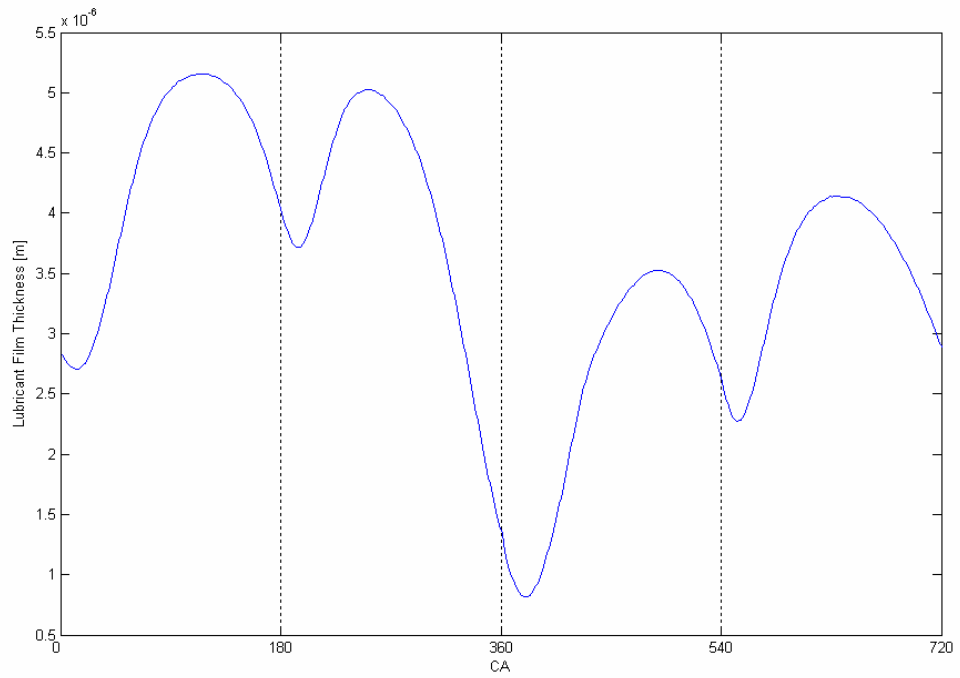
Figure 4.1 Graph of Film Thickness for Conventional Cylinder Bore

4.2.2 Triangular Dimpled Cylinder Bore Results

In Figure 4.2, the film thickness deviation for a triangular dimpled cylinder bore is shown.
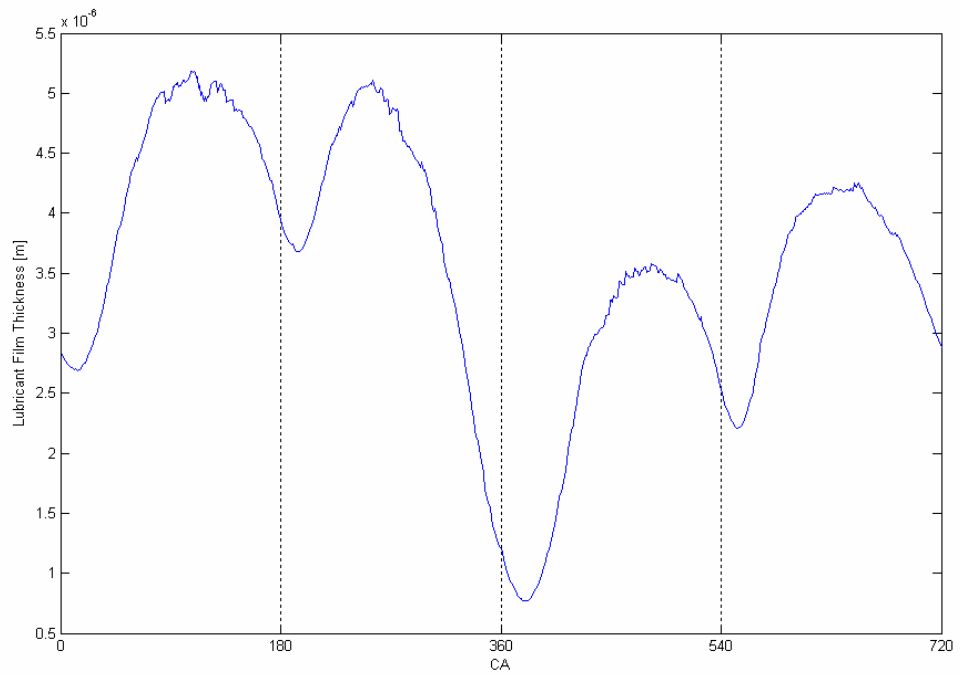
Figure 4.2 Graph of Film Thickness for Triangular Dimpled Cylinder Bore

4.2.3 Comparison of Lubricant Film Thickness Results

In Figure 4.3 the comparison of lubricant film thickness between two different cylinder bores can be seen. According to these graphs it is seen that lubricant film thickness results for triangular dimpled and conventional cylinder bores are very close to each other.
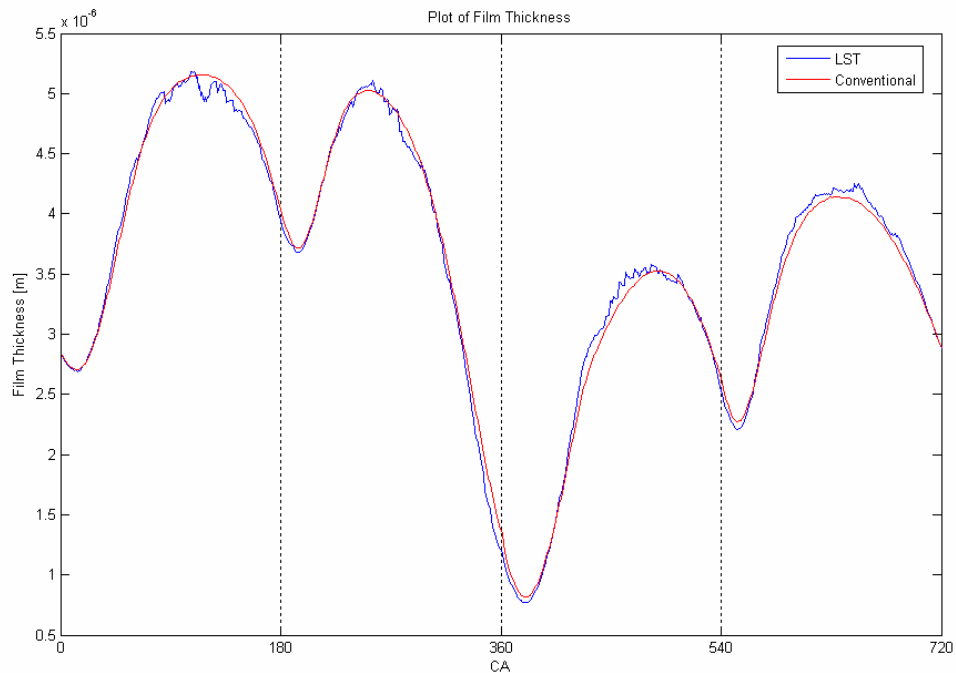
Figure 4.3 Comparisons of Film Thickness Results

As it is seen through Figure 4.3 there are some oscillations in LST cylinder bore results at the middle of the strokes where the ring moves fast. The main reason of this oscillation is seen as the higher velocity of the ring at these crankangles. Because of this high ring velocity the dimple appears and disappears in the wetted zone at two following crankangles and this causes nonlinearity at the system.

4.3. Hydrodynamic Pressure Distribution

4.3.1 Conventional Cylinder Bore Results

In Figure 4.4 and Figure 4.5 the hydrodynamic pressure distributions of conventional cylinder bore at 350 CA and 590 CA can be seen.

41
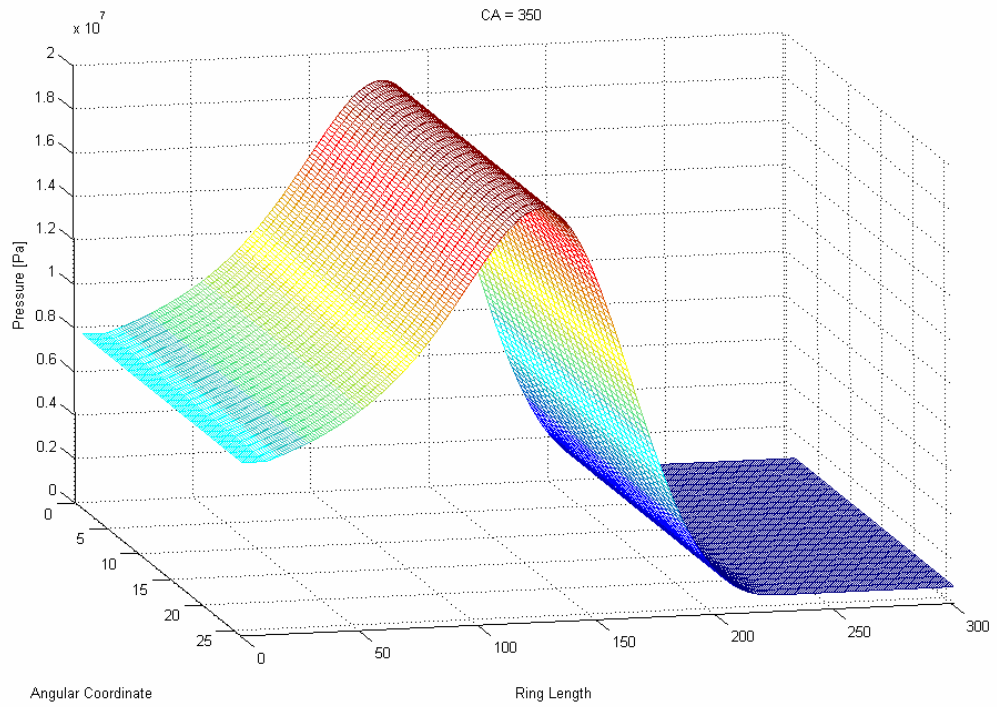
Figure 4.4 Hydrodynamic Pressure Distribution for Conventional Cylinder Bore (CA = 350)
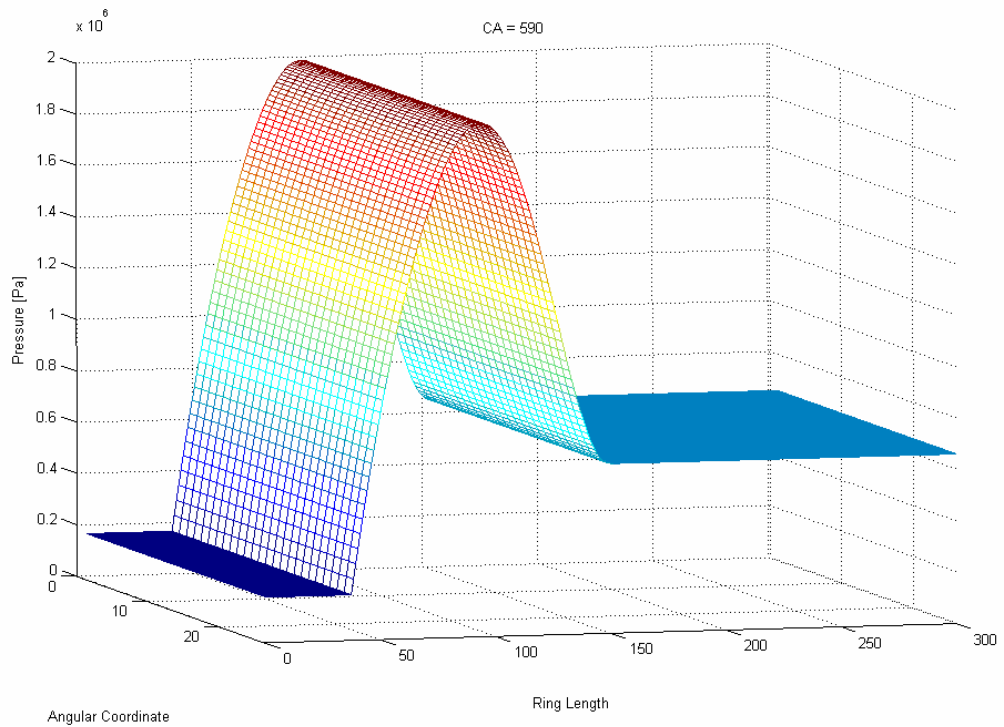
Figure 4.5 Hydrodynamic Pressure Distribution for Conventional Cylinder Bore (CA = 590)

4.3.2 Triangular Dimpled Cylinder Bore Results

In Figure 4.6 and Figure 4.7 the hydrodynamic pressure distributions of triangular dimpled cylinder bore at the same CA's can be seen.
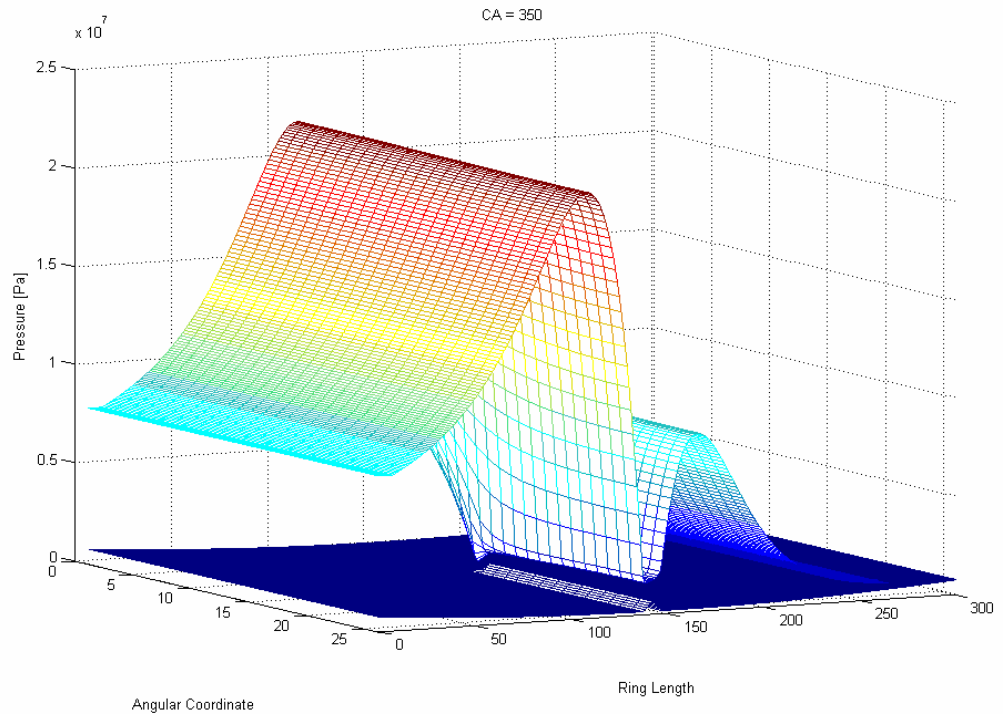
Figure 4.6 Hydrodynamic Pressure Distribution for Triangular Dimpled Cylinder Bore (CA = 350)
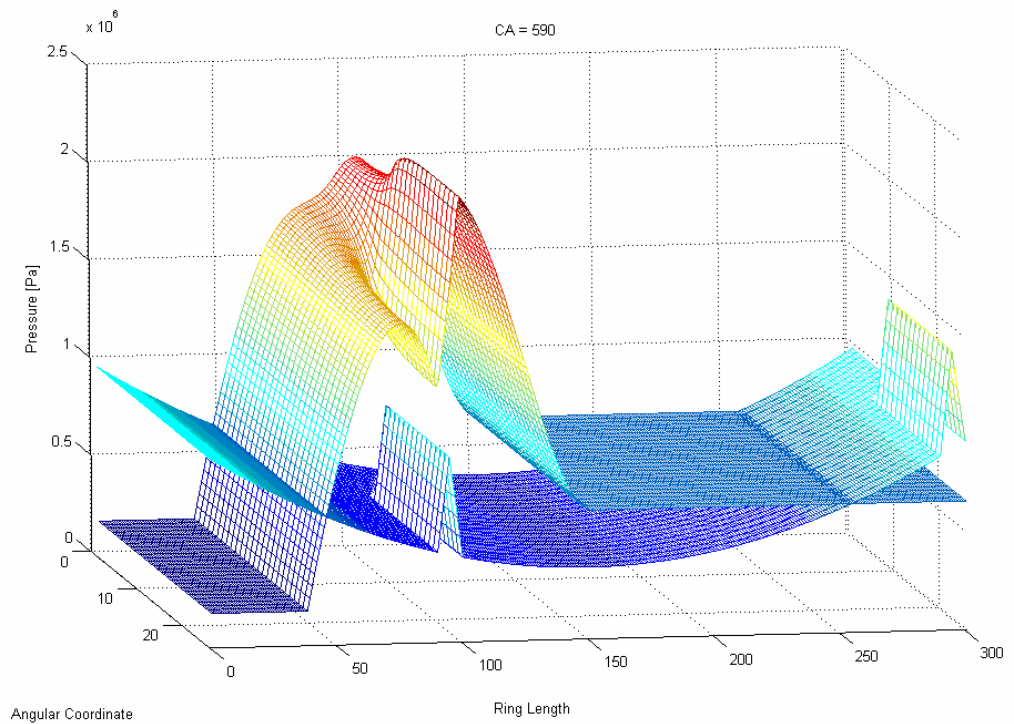
Figure 4.7 Hydrodynamic Pressure Distribution for Triangular Dimpled Cylinder Bore (CA = 590)

From hydrodynamic pressure distribution graphs it is seen that dimples causes a decrease at the local pressures of the lubricated zone.

4.3.3 Comparison of Hydrodynamic Pressure Distribution

As it is seen from Figure 4.8 and Figure 4.9 the hydrodynamic pressure for LST cylinder bore is less than the conventional cylinder bore at the dimpled section of the bore. But the load carrying capacities are not different, because of the higher pressures at the converging section of the dimple.
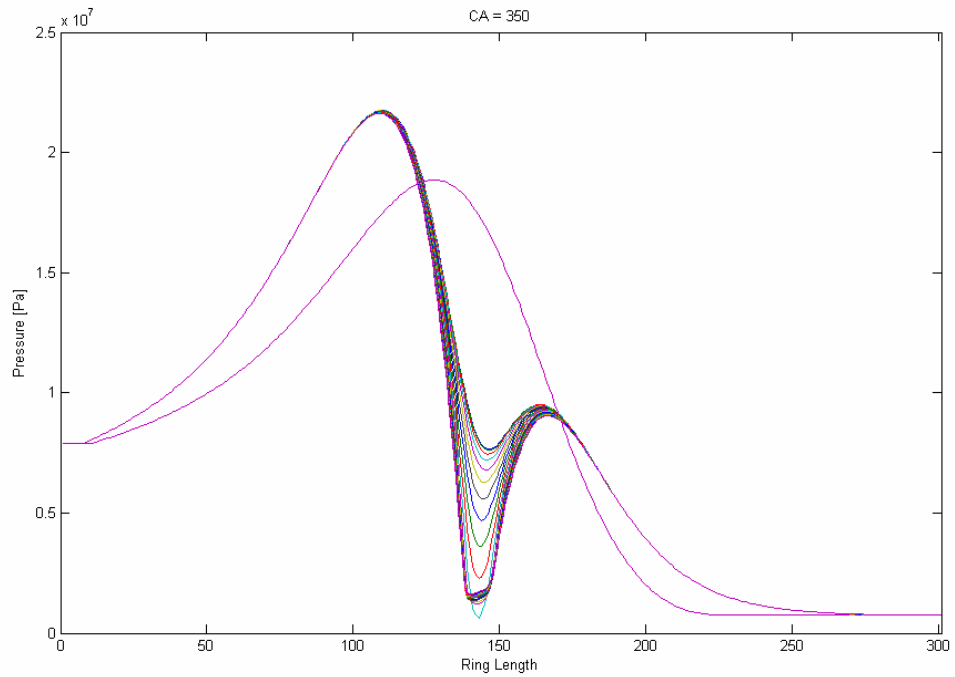
Figure 4.8 Comparison of Hydrodynamic Pressure Distribution for CA = 350
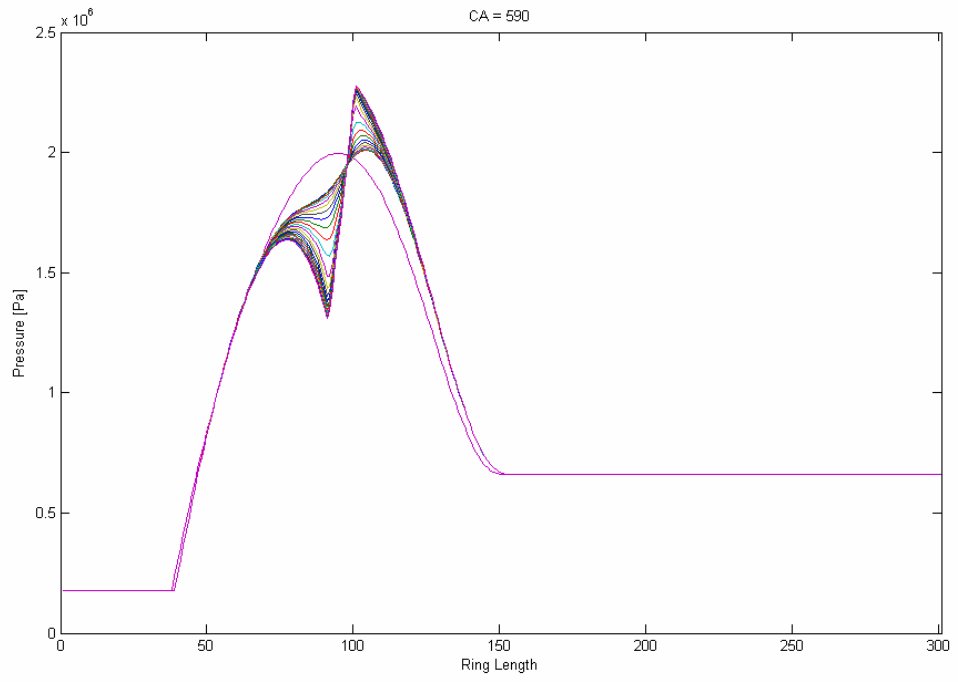
Figure 4.9 Comparison of Hydrodynamic Pressure Distribution for CA = 590

5 CONCLUSION AND FUTURE RECOMMENDATIONS

In this study, a MATLAB code was created in order to investigate the tribological performance of a piston ring which reciprocates in a laser surface textured cylinder bore. In the mathematical model, modified Reynolds equation which contains flow factors is used to add the effects of surface asperities of the ring and the bore. Furthermore, an asperity contact model was added to the program to allow it to work in both mixed and hydrodynamic lubrication regimes. Rupture of the lubricant film was solved with Reynolds boundary conditions and in order to model the small dimples on the bore, a moving bore surface was constructed and the solution was done for each crankangle.

As a result of this study, a tool was developed which can be used for dynamics of piston rings which reciprocates on a laser surface textured or conventional cylinder bore.

For the forthcoming studies, the code will be improved to solve every kind of LST specifications and dimple geometries. Also a friction model will be added to the code to calculate the change of friction force over a whole engine cycle and to see the effects of dimples on the change of friction coefficient. Also the effects of thermal and elastic deformations, which have significant effect on lubricant film thickness, will be considered in order to have more realistic results.

Also, some experimental studies will be done as an extension of this study. The experiments will be done on both a real engine and a designed test rig. On the real engine experiments, cylinder bores with different LST specifications will be used and on the bench test system experiments different LST test specimens will be used. Finally the theoretical results which are obtained from the code will be compared with the experimental results.

REFERENCES

[1] Priest, M., Taylor, C. M., 2000. Automobile Engine Tribology – Approaching the Surface, Wear, **241,** 193-203

[2] Akalın, Ö., Newaz, G., M., 2001. Piston Ring – Cylinder Bore Friction Modeling in Mixed Lubrication Regime: Part I – Analytical Results, ASME Journal of Tribology, **123,** 211-218

[3] Rohde, S. M., 1980. A Mixed Friction Model for Dynamically Loaded Contacts with Application to Piston Ring Lubrication, *Winter Annual Meeting of ASME*, Chicago, IL.

[4] Richardson, D. E., 2000. Review of Power Cylinder Friction for Diesel Engines, ASME Journal of Engineering for Gas Turbines and Power, **122,** 506-519

[5] Andersson, P., Tamminen, J., Sandström, C., E., 2002. Piston Ring Tribology – A literature Survey, VTT Technical Research Centre of Finland, Finland

[6] Yong, Z., Guohua, C., Bing, L., 1999. Two Dimensional Numerical Analysis of Piston Ring Lubrication of an Internal Combustion Engine, SAE 1999-01-1222

[7] Herbst, H., M., Priebsch, H.,H., 2000. Simulation of Piston Ring Dynamics and Their Effect on Oil Consumption, SAE 2000-01-0919

[8] Riken Corporation, 2002. Piston Ring Museum, on-line, Available from http://www.riken.co.jp/e/piston/c/c_3.html

[9] Etsion, I., 2005. State of Art in Laser Surface Texturing, ASME Journal of Tribology, **127,** 248-253

[10] Herbst, L., Lindner, H., Heglin, M., Hoult, T., 2004. Targeting Diesel Engine Efficiency, Industrial Laser Solutions, Application Report

[11] Gehring GmbH & Co. KG, 2004. The Future of the Surface – Optimum Tribosystems through Functionally Optimized Surfaces, Technical Brochure

[12] **Herbst, L., Lindner, H., Hoult, T.,** 2004. An Important Novel Application for Excimer Lasers in the Automotive Industry, *23rd International Congress on Applications of Lasers & Electro – Optics,* October 7th

[13] **Klink, V.U.,** 1997. Laserhonen fur Zylinderlaufbahnen MTZ Motortechnische Zeitschrift, **58,** 554-556

[14] **Wang, Q. J., Zhu, D.,** 2004. Virtual Texturing: Modeling the Performance of Lubricated Contacts of Engineered Surfaces, ASME Journal of Tribology, **127,** 722-728

[15] **Feldman, Y., Kligerman, Y., Etsion, I., Haber, S.,** 2006. The Validity of the Reynolds Equation in Modeling Hydrostatic Effects in Gas Lubricated Textured Parallel Surfaces, ASME Journal of Tribology, **128**, 345-350

[16] **Ronen, A., Etsion, I., Kligerman,. Y.,** 2001. Friction Reducing Surface Texturing in Reciprocating Automotive Components, Tribology Transactions, **44**, 359-366

[17] **Kligerman, Y., Etsion, I., Shinkarenko, A.,** 2005. Improving Tribological Performance of Piston Rings by Partial Surface Texturing, ASME Journal of Tribology, **127**, 632-638

[18] **Feldman, Y., Kligerman, Y., Etsion, I.,** 2006. A hydrostatic laser surface textured gas seal, Tribology Letters

[19] **Kligerman, Y., Etsion, I.,** 2001. Analysis of the Hydrodynamic Effects in a Surface Textured Circumferential Gas Seal, Tribology Transactions, **44**, 472-478

[20] **Brizmer, V., Kligerman, Y., Etsion, I.,** 2003. A Laser Surface Textured Parallel Thrust Bearing, Tribology Transactions, **46**, 397-403

[21] **Siripuram, R. B., Stephens, L. S.,** 2004. Effect of Deterministic Asperity Geometry on Hydrodynamic Lubrication, ASME Journal of Tribology, **126**, 527-534

[22] **Ryk, G., Kligerman, Y., Etsion, I.,** 2002. Experimental Investigation of Laser Surface Texturing for Reciprocating Automotive Components, Tribology Transactions, **45**, 444-449

[23] **Etsion, I., Halperin, G., Brizmer, V., Kligerman, Y.,** 2004. Experimental Investigation of Laser Surface Textured Parallel Thrust Bearings, Tribology Letters, **17**, 295-300

[24] Ryk, G., Kligerman, Y., Etsion, I., Shinkarenko, A., 2005. Experimental Investigation of Partial Laser Surface Texturing for Piston – Ring Friction Reduction, Tribology Transactions, **48,** 583-588

[25] Kovalchenko, A., Ajayi, O., Erdemir, A., Fenske, G., Etsion, I., 2005. The Effect of Laser Surface Texturing on Transitions in Lubrication Regimes During Unidirectional Sliding Contact, Tribology International, **38**, 219-225

[26] Wakuda, M., Yamauchi, Y., Kanzaki, S., Yasuda, Y., 2003. Effect of Surface Texturing on Friction Reduction between Ceramic and Steel Materials under Lubricated Sliding Contact, Wear, **254**, 356-363

[27] Mourier, L., Mazuyer, D., Lubrecht, A. A., Donnet, C., 2006. Transient Increase of Film Thickness in Micro – Textured EHL Contacts, Tribology International, **39**, 1745-1756

[28] Kovalchenko, A., Ajayi, O., Erdemir, A., Fenske, G., Etsion, I., 2004. The Effect of Laser Texturing of Steel Surfaces and Speed Load Parameters on the Transition of Lubrication Regime from Boundary to Hydrodynamic, Tribology Transactions, **47**, 299-307

[29] Etsion, I., Halperin, G., 2002. A Laser Surface Textured Hydrostatic Mechanical Seal, Tribology Transactions, **45,** 430-434

[30] Bhushan B., 2001. Modern Tribology Handbook Volume II, CRC Press, Boca Raton

[31] Stachowiak, G., W., Batchelor, A., W., 2001. Engineering Tribology, Butterworth Heinemann

[32] Hutchings, I., M., 1992. Tribology: Friction and Wear of Engineering Materials, Hodder & Stoughton

[33] Priest, M., Dowson, D., Taylor, C., M., 2000. Theoretical Modeling of Cavitation in Piston Ring Lubrication, Proc. Instn. Mech. Eng., **214,** 435-447

[34] Dellis, P., Arcoumanis, C., 2004. Cavitation Development in the Lubricant Film of a Reciprocating Piston – Ring Assembly, Journal of Engineering Tribology, **218,** 157-171

[35] Patir, N., Cheng, H. S., 1978. An Average Flow Model for Determining Effects of Three – Dimensional Roughness on Partial Hydrodynamic Lubrication, ASME Journal of Lubrication Technology, **100,** 12-17

[36] Patir, N., Cheng, H. S., 1979. Application of Average Flow Model to Lubrication between Rough Sliding Surfaces, ASME Journal of Lubrication Technology, **101,** 220-230

[37] Greenwood, I. A., Tripp, J. H., 1971. The Contact of Two Nominally Flat Surfaces, Proc. IMechE. **185,** 625-633

[38] Hu, Y., Cheng, H. S., Arai, T., Kobayashi, Y., Aoyama, S., 1994. Numerical Simulation of Piston Ring in Mixed Lubrication – A Non – Axi – Symmetrical Analysis, ASME Journal of Tribology, **116,** 470-478

[39] Wu, C., Zheng, L., 1989. An Average Reynolds Equation for Partial Film Lubrication with a Contact Factor, ASME Journal of Tribology, **111,** 188-191

[40] Zottin, W., Peixoto, V. J. M., 2003. Numerical Simulation of Piston Rings Instability, SAE 2003-01-0981

General Mesh for Piston Ring Surface
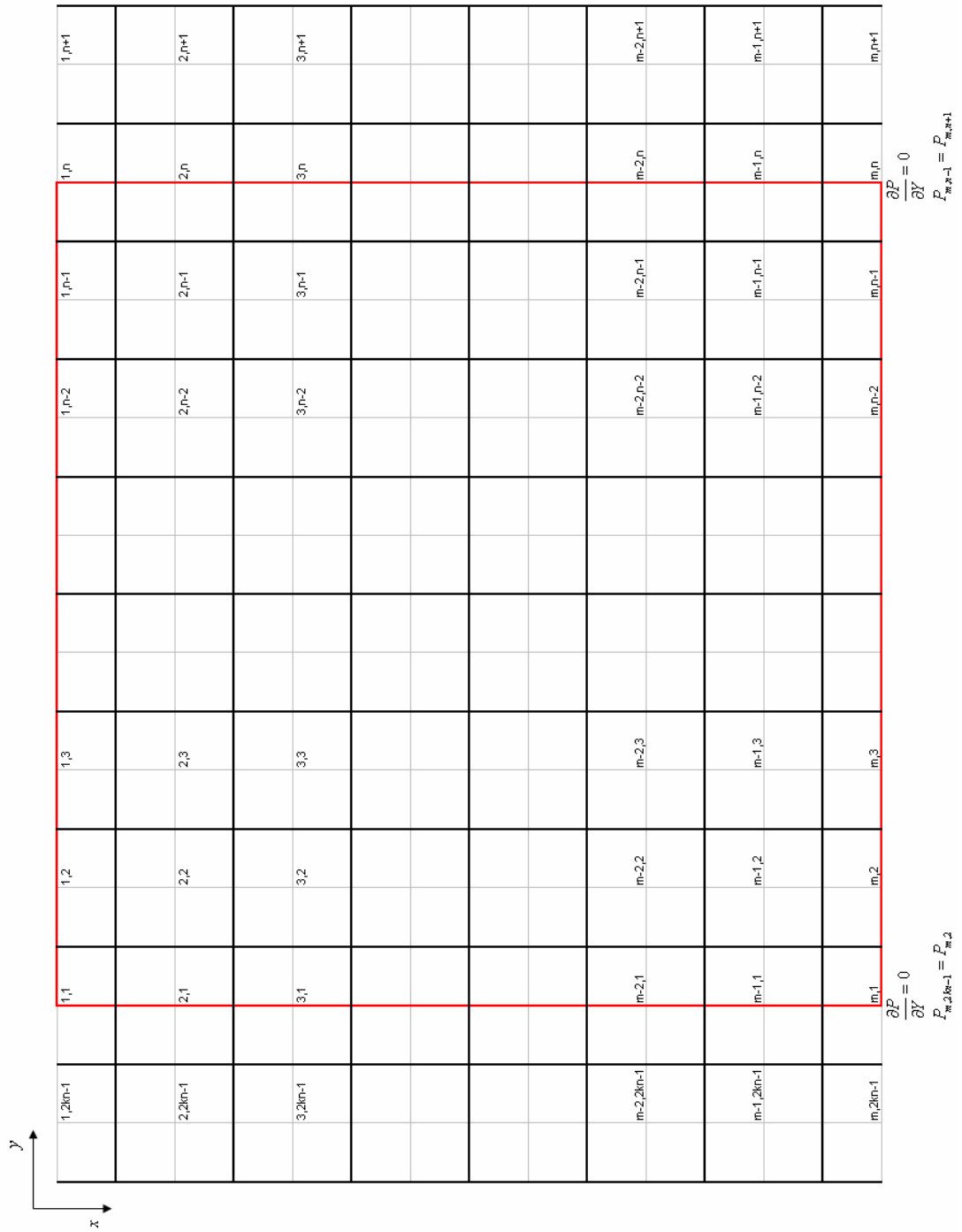
APPENDIX B

Flow Chart for the MATLAB Code

```
┌─────────────────────────────────────────────────────────────┐
│                    ┌──────────────────┐                      │
│                    │      INPUT        │                      │
│                    └──────────────────┘                      │
│                             │                                 │
│          ┌──────────────────▼──────────────┐                 │
│          │      CRANKANGLE ITERATION        │                 │
│          └──────────────────┬──────────────┘                 │
│                             │                                 │
│        ┌────────────────────▼─────────────────────┐          │
│        │  CALCULATION OF THE RING AXIAL VELOCITY   │          │
│        └────────────────────┬─────────────────────┘          │
│                             │                                 │
│            ┌────────────────▼──────────────┐                 │
│            │    BORE DOMAIN FORMATION       │                 │
│            └────────────────┬──────────────┘                 │
│                             │                                 │
│          ┌──────────────────▼──────────────┐                 │
│          │        FORCE ITERATION           │                 │
│          └──────────────────┬──────────────┘                 │
│                             │                                 │
│           ┌─────────────────▼────────────────┐               │
│           │   FILM THICKNESS CALCULATION      │               │
│           └─────────────────┬────────────────┘               │
│                             │                                 │
│       ┌─────────────────────▼──────────────────────┐         │
│       │  CALCULATION OF φx, φy, φs, φc               │         │
│       └─────────────────────┬──────────────────────┘         │
│                             │                                 │
│     ┌───────────────────────▼──────────────────────┐         │
│     │    SOLUTION OF THE MODIFIED REYNOLDS          │         │
│     │    EQUATION & CAVITATION ITERATION            │         │
│     └───────────────────────┬──────────────────────┘         │
│                          ERROR<ε                              │
│   ERROR>ε      ┌────────────▼──────────────┐                 │
│               │   PRESSURE ERROR CHECK      │                 │
│               └────────────┬──────────────┘                 │
│                             │                                 │
│          ┌──────────────────▼──────────────┐                 │
│          │   CALCULATION OF THE FORCES      │                 │
│          └──────────────────┬──────────────┘                 │
│   ERROR>ε       ┌───────────▼──────────────┐                 │
│                │    FORCE ERROR CHECK       │                 │
│                └───────────┬──────────────┘                 │
│                          ERROR<ε                              │
│        ┌───────────────────▼─────────────────────┐           │
│        │   CALCULATION OF THE NOMINAL             │           │
│        │   CLEARANCE FOR NEXT CRANKANGLE          │           │
│        └───────────────────┬─────────────────────┘           │
│                             │                                 │
│            ┌────────────────▼──────────────┐                 │
│            │      NEXT CRANKANGLE           │                 │
│            └───────────────────────────────┘                 │
└─────────────────────────────────────────────────────────────┘
```

APPENDIX C

Table C.1 Parameters for Pressure Flow Factor

γ	C	R	Range
1/9	1.48	0.42	H>1
1/6	1.38	0.42	H>1
1/3	1.18	0.42	H>0.75
1	0.90	0.56	H>0.5
3	0.225	1.5	H>0.5
6	0.520	1.5	H>0.5
9	0.870	1.5	H>0.5

Table C.2 Parameters for Shear Flow Factor

γ	A_1	α_1	α_2	α_3	A_2
1/9	2.046	1.12	0.78	0.03	1.856
1/6	1.962	1.08	0.77	0.03	1.754
1/3	1.858	1.01	0.76	0.03	1.561
1	1.899	0.98	0.92	0.05	1.126
3	1.560	0.85	1.13	0.08	0.556
6	1.290	0.62	1.09	0.08	0.338
9	1.011	0.54	1.07	0.08	0.295

CURRICULUM VITAE

The author was born in Akhisar, Manisa, in 1982. He graduated from Eskişehir Fatih High School of Science in 2000 and started his undergraduate education at the mechanical engineering faculty of İstanbul Technical University. He completed his undergraduate education in 2005 and at the same year he started his M.Sc. education at the automotive division of the same faculty. He started to work as a research assistant during his M.Sc. education at the division and received his M.Sc. degree in 2007. He is still working as a research assistant at the automotive division of mechanical engineering faculty of İstanbul Technical University.